JGR Oceans

RESEARCH ARTICLE
10.1029/2022JC018431

North-South Differences in Under-Ice Primary Production in the Chukchi Sea From 1988 to 2018

C. M. Payne[1], G. L. van Dijken[1], and K. R. Arrigo[1]

[1]Department of Earth System Science, Stanford University, Stanford, CA, USA

Key Points:

- Under-ice blooms (UIBs) diminished over time in the southern Chukchi Sea, indicating reduced impact to future Chukchi Sea biogeochemistry
- In the north, years with high net primary production (NPP) feature massive UIBs; in the south, years with higher NPP do not have UIBs
- Modeled NPP, particle export and sedimentary denitrification are greater in the southern Chukchi Sea than in the north

Supporting Information:

Supporting Information may be found in the online version of this article.

Correspondence to:

C. M. Payne,
cmpayne@stanford.edu

Citation:

Payne, C. M., van Dijken, G. L., & Arrigo, K. R. (2022). North-south differences in under-ice primary production in the Chukchi Sea from 1988 to 2018. *Journal of Geophysical Research: Oceans*, *127*, e2022JC018431. https://doi.org/10.1029/2022JC018431

Received 18 JAN 2022
Accepted 22 JUN 2022

Abstract As Arctic sea ice has thinned and begun to retreat earlier in the year, there have been substantial changes in the timing and magnitude of regional net primary production (NPP). Most notably, field, remote sensing, and model-based studies have demonstrated that massive under-ice phytoplankton blooms (UIBs) contribute substantially to annual NPP and can even drive increases in sedimentary nitrogen recycling and loss through coupled partial nitrification-denitrification. In this study, we used a 1-D biogeochemical model (CAOS-GO) to compare the magnitude of NPP associated with UIBs in the northern and southern Chukchi Sea between 1988 and 2018. While UIBs were critical in driving interannual variation and secular increases in annual NPP and sedimentary nitrification and denitrification in the northern Chukchi Sea, UIBs were far less important at our southern site. As the length of the under-ice (UI) period diminished between 1988 and 2018 in the southern Chukchi Sea, there was a decrease in the amount of NPP produced during the UI period. Despite higher rates of both annual NPP and denitrification at the southern site, there were no secular trends in these rates over time. Our results indicate that, as sea ice continues to retreat earlier, the impact of UIBs on the biogeochemistry of the Chukchi Sea is likely to diminish.

Plain Language Summary Historically, sea ice coverage was assumed to prevent most phytoplankton production in the Chukchi Sea sector of the western Arctic Ocean. However, changes in sea ice thickness and the proliferation of melt ponds on the surface of the sea ice have allowed massive under-ice phytoplankton blooms (UIBs) to form. Here, we used a 1-D biogeochemical model (CAOS-GO) to compare the magnitude of NPP associated with UIBs in the northern and southern Chukchi Sea between 1988 and 2018. In the northern Chukchi Sea, UIBs can contribute substantially to annual phytoplankton production and can even increase the rate of nitrogen recycling and loss in the sediments. However, in the southern Chukchi Sea, the under-ice period shortened between 1988 and 2018 and UIBs shrunk in magnitude. While the southern Chukchi Sea hosted overall higher rates of production and sedimentary N loss, these did not show a trend over time. Our results indicate that, as sea ice continues to retreat earlier, the impact of UIBs on the biogeochemistry of the Chukchi Sea is likely to diminish.

1. Introduction

A substantial decline in sea ice extent and thickness has been observed throughout the Arctic Ocean (Kwok, 2018; Serreze & Stroeve, 2015). Air and sea surface temperatures (SSTs) in the Arctic are warming disproportionately compared to the global average (Stocker et al., 2013). This is especially true in the Chukchi Sea, which extends westward from the coast of Alaska to Russia. The Chukchi Sea is warming more rapidly than most of the Arctic Ocean (Richter-Menge et al., 2019), contributing to a 33 day increase in the length of the Chukchi Sea open water (OW) period between 2009 and 2018 (Lewis et al., 2020). Model projections indicate that the OW period will increase to 6–7 months by 2040 in the southern Chukchi Sea, representing a 100% increase from the present 3–4 months (Wang & Overland, 2015). Additionally, the Arctic Ocean has experienced significant declines in multiyear ice, which covered nearly 60% of the Arctic Ocean in 1988 (Serreze & Stroeve, 2015) but less than 30% of the Arctic Ocean by 2017 (Kwok, 2018). Much of the Chukchi Sea is now covered by far thinner first-year ice; between 1958 and 2017, average sea ice thickness declined by 70%, from 2 to 0.6 m (Kwok, 2018).

The increasing length of the OW period and the thinner sea ice cover have had substantial effects on primary producers in the Chukchi Sea. Net primary production (NPP) increased by 96% between 1998 and 2018 thanks in part to the increase in the length of the OW period (Lewis et al., 2020). Further, a satellite study by Ardyna et al. (2014) indicates that between 1998 and 2012 there was a 35% increase in the incidence of autumn blooms in the Chukchi

Sea, although this effect was patchy across the region. In addition to changes in NPP during the OW period, the observation of massive under-ice blooms (UIBs; Arrigo et al., 2012, 2014; Hill, Ardyna, et al., 2018) in the Chukchi Sea has upset the paradigm that most Arctic Ocean NPP is generated in the marginal ice zone (MIZ; Perrette et al., 2011). Phytoplankton biomass can exceed 1,000 mg chlorophyll *a* (Chl *a*) m^{-2} (Arrigo et al., 2014) during the under-ice (UI) period even under fully consolidated 1 m thick sea ice. Satellite analysis and modeling studies indicate that Chukchi Sea UIBs are more common than MIZ-generated blooms (Lowry et al., 2014) and could have been a feature of the Arctic Ocean since at least the late 1980s (Clement Kinney et al., 2020; Horvat et al., 2017; Jin et al., 2016; Payne et al., 2021; Zhang et al., 2015).

Changes in sea ice conditions and the timing and magnitude of annual NPP likely impact the marine nitrogen (N) cycle in the Chukchi Sea and in downstream ecosystems (Arrigo et al., 2014; Arrigo & Van Dijken, 2015). The diatom blooms that predominate in the Chukchi Sea (Laney & Sosik, 2014) can sink rapidly to the seafloor due to the large cell size and silicified cell walls (Smetacek, 1999), disproportionately exporting particulate organic carbon (POC) out of the surface ocean. But UIBs might allow even higher rates of POC export to the sediments because of the low grazing rates (Campbell et al., 2001; Sherr & Sherr, 2009; Sherr et al., 2009) associated with the cold water temperatures (−1.5°C) found during this period. As NPP has increased in the northern Chukchi Sea, particulate export to the sediments has likely increased (Payne & Arrigo, 2022). On the broad continental shelf of the Chukchi Sea, coupled partial nitrification-denitrification in the sediments leads to high N recycling and loss (Brown et al., 2015), causing the region to contribute 1%–3% of the total N lost in the world's oceans (Chang & Devol, 2009). An increase in the rate of POC export can subsequently lead to increases in the loss of fixed N from the system (Payne & Arrigo, 2022), reducing the amount of N available to primary producers downstream (Arrigo & Van Dijken, 2015).

Here, we use the Coupled Arctic Ocean Sediment model with GOTM and OMEXDIA (CAOS-GO; Figure S1 in Supporting Information S1) to assess how changes in NPP and the N cycle may have differed between the northern and southern Chukchi Sea from 1988 to 2018. The model is composed of interconnected physical, biogeochemical, and sedimentary chemistry models. CAOS-GO was previously implemented in the northern Chukchi Sea (Payne & Arrigo, 2022; Payne et al., 2021) at a location where UIBs were observed by Arrigo et al. (2014). This northern site was located 100 km south of the northern edge of the Chukchi shelf and was covered by multi-year ice in some years and first-year ice in others (Payne et al., 2021). However, first-year ice dominates over much of the rest of the Chukchi Sea and sea ice retreats earlier in the year in the south than it does in the north (Richter-Menge et al., 2019). As a result of the very different ice conditions, SSTs in the southern Chukchi Sea have changed substantially more rapidly than to the north, increasing to as high as 11°C in the southern Chukchi Sea in August of 2018 (Osborne et al., 2018). Here, we compare the NPP previously projected in the northern Chukchi Sea (Payne et al., 2021) to the southern Chukchi Sea and identify the environmental variables that control NPP during the UI, MIZ, and OW periods. In addition, we evaluate how export of particulate organic N (PON) to the benthos, nitrification in the water column and sediments, and sedimentary denitrification may have changed between 1988 and 2018 in the southern Chukchi Sea and how this compares to the northern Chukchi Sea (Payne & Arrigo, 2022).

2. Methods

2.1. Modeling Configuration

The coupled CAOS-GO model (Figure S1 in Supporting Information S1) was implemented in the southern Chukchi Sea at 67.78°N and 168.24°W (station 3.7 of the Distributed Biological Observatory; Moore & Grebmeier, 2018) and in the northern Chukchi Sea at 72.16°N and 166.60°W (Figure 1; Payne & Arrigo, 2022; Payne et al., 2021) for the years 1988–2018. Hereafter, we refer to the northern model location as the north and the southern model location as the south.

The physical component of CAOS-GO, the General Ocean Turbulence Model (GOTM, version 5.4; Burchard et al., 1999), was used to produce hourly profiles of temperature, salinity, buoyancy frequency, and turbulent diffusion coefficients. The biogeochemical model, CAOS (Payne et al., 2021), dynamically simulates the vertical behavior of N-based state variables in sea ice and over a 50 m water column, including ice algae, small and

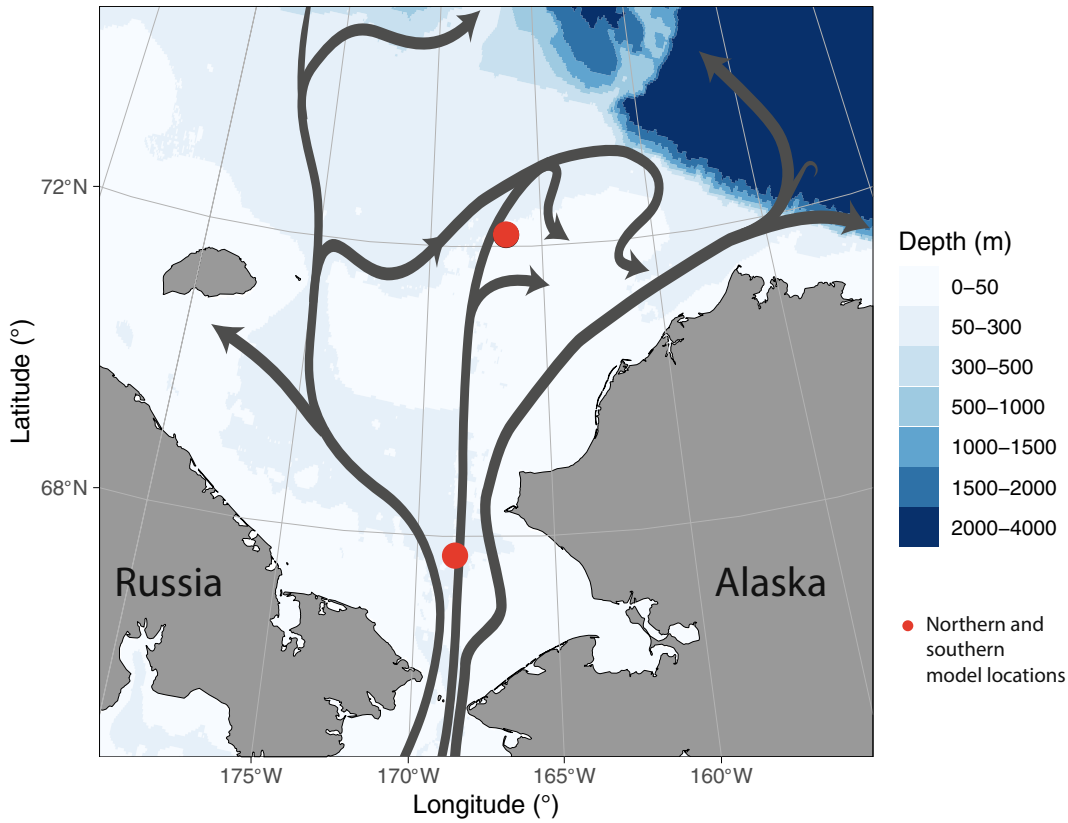

Figure 1. Bathymetric map of the Chukchi Sea including schematic flow paths of advected water (gray lines, after Corlett & Pickart, 2017). Red points represent the southern and northern model locations.

large phytoplankton (representing flagellates and diatoms, respectively), small and large zooplankton (representing phagotrophic protists and large copepods, respectively), nitrate (NO_3^-), ammonium (NH_4^+), and detritus. Initial concentrations of these N-based state variables are described in Table 1, while the effects of advection are simulated by relaxing all N-based state variables toward prescribed profiles. Because water in the Chukchi Sea advects from the south, where sea ice cover diminishes earlier, phytoplankton growth in these advecting waters begins earlier and will have slightly higher phytoplankton and lower nutrient concentrations than at our model location. We generated these prescribed profiles by running the model twice. As in Payne et al. (2021), model profiles generated for Day+1 (first run) were used as prescribed profiles for Day+0 (second run). NO_3^- profiles were further modified following DOY 300 to gradually increase back to the initial NO_3^- concentration (Table 1). The sediment model, OMEXDIA (Soetaert et al., 1996a, 1996b), calculates changes in fast- and slow-remineralizing organic matter, oxygen (O_2), NO_3^-, NH_4^+, N_2, and a reduced substances state variable using Chukchi Sea-specific parameters (Table 2). Inputs to OMEXDIA include bottom-water NO_3^- and NH_4^+ concentrations and rates of particulate organic N (PON) export to the benthos from CAOS and inputs of bottom-water temperature and salinity from GOTM. OMEXDIA calculates rates of nitrification and denitrification as well as the fluxes of NO_3^- and NH_4^+ between the sediments and the water column that are used as inputs to CAOS.

Model inputs for CAOS-GO include both satellite-derived and reanalysis data that characterize atmospheric conditions, albedo, idealized temperature and salinity profiles, sea ice concentration and age, and cloud-adjusted

Table 1
State Variables and Initial Values for the CAOS model.

State variable	Description	Initial value
IA	Ice algae	0.01
Sphy	Small phytoplankton functional group	0.05[a]
Lphy	Large phytoplankton functional group	0.05[a]
Szoo	Small zooplankton functional group	0.01[a]
Lzoo	Small zooplankton functional group	0.01[a]
Detri	Detritus functional group	0.0
NO_3^-	Dissolved nitrate concentration	16.0
NH_4^+	Dissolved ammonium concentration	0.0

Note. All are in units of mmol N m^{-3}.
[a]indicates that the initial value is also a minimum value. From Payne et al. (2021).

Table 2
Parameters (including values, units, and original sources) Used in the OMEXDIA Model That Differ From Those in Soetaert et al. (1996b)

Parameter	Description	Value	Unit	Source
F_{fast}	Flux of fast-decaying detritus	(*)	g C m^{-2} yr^{-1}	a
F_{slow}	Flux of slow-decaying detritus	(*)	g C m^{-2} yr^{-1}	a
p_{fast}	Proportion of fast-decaying detritus	0.5	d^{-1}	b
R_{fast}	Decay rate for the fast-decaying detritus	0.18	d^{-1}	c
R_{slow}	Decay rate for the slow-decaying detritus	0.005	d^{-1}	b
$k_{in}(O_2$ denit)	Half saturation conc. for O_2 inhibition of denitrification	15	mmol O_2 m^{-3}	d
$k_{in}(NO_3^-$ anox)	Half saturation conc. for NO_3^- inhibition of anoxic mineralization	1	mmol NO_3^- m^{-3}	d
$k_{in}(O_2$ anox)	Half saturation conc. for O_2 inhibition of anoxic mineralization	1	mmol NO_3^- m^{-3}	d
C/N_{fast}	Carbon to nitrogen ratio of fast-decaying detritus	106/14.18	mol:mol	a
C/N_{slow}	Carbon to nitrogen ratio of slow-decaying detritus	106/12.1	mol:mol	e
ϕ_0	Porosity at the sediment-water interface	0.915	-	d
$coeff_\phi$	Coefficient for exponential porosity changes	4	-	b
Db_0	Constant bioturbation coefficient in the bioturbated layer	2	cm^2 yr^{-1}	f
x_b	Depth below which bioturbation decays exponentially	3	cm	f
O_2_bw	Oxygen concentration of the bottom water NO_3^-	300	mmol N m^{-3}	**
NO_3^-_bw	Daily mean bottom-water NO_3^-	(*)	mmol N m^{-3}	a
NH_4^+_bw	Daily mean bottom-water NH_4^+	(*)	mmol N m^{-3}	a
w	Sedimentation rate	0.12	cm y^{-1}	e
Temperature	Daily mean bottom-water temperature	(*)	°C	a
Salinity	Daily mean bottom-water salinity	(*)	-	a

Note. From Payne et al. (2021). (*) Variable conditions produced by GOTM or the CAOS model. **Mean oxygen concentration for the stations closest to the model location for ICESCAPE 2011.

[a]From CAOS model. [b]Soetaert et al. (1996b). [c]Davis and Benner (2007). [d]Soetaert et al. (1996a). [e]Cooper and Grebmeier (2018). [f]Teal et al. (2008).

surface irradiance. For further details on model inputs, see Payne et al. (2021). See Supporting Sections S2 and S3 in Supporting Information S1 for details about model validation at the southern model location.

2.2. Physical Model Configuration

As in Payne et al. (2021), horizontal advection, precipitation, and sea ice melt were not directly included in our GOTM setup. To compensate for these processes, modeled salinity and temperature profiles were relaxed toward idealized profiles on timescales of 5 and 15 days, respectively. Idealized profiles were created for each year by using remote sensing products and cruise data collected between 2010 and 2018 (Arrigo et al., 2014; Grebmeier, 2017; Pacini et al., 2019; Peralta-Ferriz & Woodgate, 2015) as well as modeled fields (Maslowski et al., 2004). The same idealized wintertime temperature and salinity profiles were used each year (Pacini et al., 2019). Subsequently, to reflect interannual differences in the timing of sea ice retreat, idealized temperature profiles in the spring and summer varied based on sea ice concentration as well as satellite-derived SST. The salinity in the mixed layer for each year's idealized profiles was scaled depending on the length of the sea ice melt period to reflect annual differences in freshwater input to the water column. As in Payne et al. (2021), local sea ice melt generated 50% of the salinity changes in these idealized profiles, with the remaining 50% presumed to be generated by horizontal advection of sea ice melt, precipitation, and runoff. For more details, see Supplemental Section S1 in Supporting Information S1.

2.3. Primary Production

Microalgal primary production was divided into four periods each year: the ice algal (IA), UI, MIZ, and OW periods. The first of these periods, the IA period, started when light at the top of the sea ice algal layer increased

above a compensation irradiance of 2 μmol photons m^{-2} s^{-1} (McMinn et al., 1999). This period ended on the ice melt date, when air temperatures rose above 0°C for 24 hr—see Payne et al., 2021 and ice algae were presumed to slough off the bottom of the sea ice. The UI period started when phytoplankton growth began (defined as the date when daily phytoplankton NPP exceeded 0.05 g C m^{-2} d^{-1}) and continued until the start of sea ice retreat, when satellite-derived sea ice concentration diminished below 90%. The third period, the MIZ period, stretched from the start to the end of sea ice retreat (when sea ice concentrations diminished below 10%). Finally, the OW period extended from the end of sea ice retreat to either the date that sea ice began to advance in the autumn or when average mixed layer light diminished below 2 μmol photons m^{-2} s^{-1}, whichever was earliest.

NPP was also categorized as new or regenerated and surface or subsurface production. New production was driven by NO_3^- utilization, while regenerated production was driven by NH_4^+ utilization. To determine the NPP generated in the surface or subsurface, large phytoplankton biomass for each layer (z) of the water column below 10 m was compared to the layer above ($z-1$). If the lower layer (z) had 10% more biomass than the layer above ($z-1$), that layer was considered to be the upper boundary of the subsurface Chl *a* maximum (SCM). Total NPP above that depth was then defined as surface NPP, while NPP at or below that depth was defined as NPP within the SCM. If no obvious SCM existed (z always had <10% more biomass than $z-1$), integrated water column NPP was considered surface NPP.

2.4. Statistics

We evaluated the importance of environmental conditions (e.g., ice thickness, length of UI period) on NPP, PON export, and nitrification and denitrification, using multiple linear regression analysis. We checked for collinearity among predictor variables by using the variance inflation factor (VIF), but found only moderate correlation (VIF was <3.5 for all variables). Backward selection was used to identify multiple linear regressions. In backward selection, the variable with the highest p-value was sequentially eliminated until only statistically significant ($p < 0.05$) variables remained. Regressions were subsequently checked using visual inspection of histograms, quantile-quantile plots, and plots of the independent and dependent variables and the Shapiro-Wilk test. Linear regressions are reported with the standard error, and plots with linear regressions include a confidence interval of 95%. Relative importance of each variable in multiple linear regressions was assessed using the "relaimpo" statistical package in *R*, version 2.2-6 (Grömping, 2006).

Annual cycles of daily NPP were clustered into distinct water column bloom types using *k*-means clustering based on NPP in the UI and MIZ periods. The optimal k value was determined using the gap statistic. To quantify the relationship between water column bloom type and NPP, PON export to the benthos, nitrification, and denitrification, ANOVA and post hoc Tukey's honest significant difference tests were used. Statistical analyses were all conducted in *R* version 4.1.0.

3. Results

3.1. Snow and Ice Conditions

Satellite-derived snow and ice conditions differed significantly between the southern and northern Chukchi Sea. While the north typically featured multiyear sea ice, the south exclusively hosted thinner first-year ice with a snow cover that was only two thirds as thick as that in the north (Figures 2a–2c and Table 3). Snow started melting 4 weeks earlier in the south, allowing IA blooms to start 1 month earlier (in mid-March) and last 3 weeks longer than in the north (Figures 2d, 3a and Table 3). Sea ice retreat also started 40 days earlier and ended 53 days earlier in the south (typically stretching from mid-May to early June between 1988 and 2018) than in the north (where sea ice retreat streted from the end of June to the end of July; Figures 2f, 2g and Table 3). This early sea ice retreat in the southern Chukchi Sea caused both shorter UI and MIZ periods than in the north by 14 and 13 days, respectively (Figures 3b, 3c and Table 3). In both the south and the north, ice retreat shifted to earlier in the year between 1988 and 2018 (Table 4). This resulted in a UI period in the southern Chukchi Sea that shortened by 7.0 d per decade between 1988 and 2018. Sea ice advance began later over time in both the south and the north (Table 4), advancing on average 16 days later in the south than in the north (Figure 2h and Table 3). The south typically had a 42 days longer OW period than the north (Figure 3d and Table 3), although this diminished over time, since the OW period lengthened more rapidly in the north than in the south (Table 4).

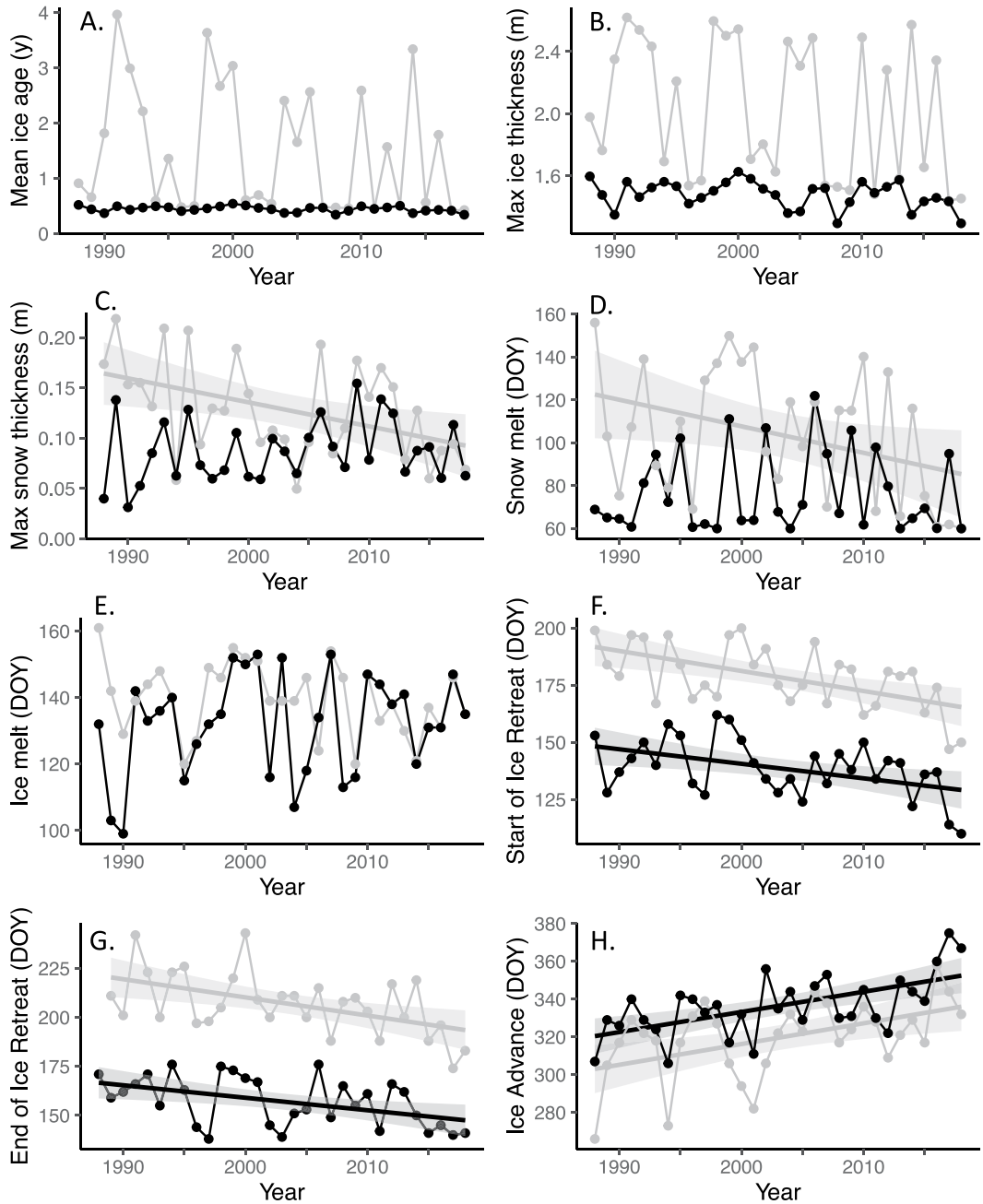

Figure 2. Ice and snow conditions between 1988 and 2018: (a) mean ice age (y), (b) maximum ice thickness (m), (c) maximum snow thickness (m), (d) snow melt date (DOY), (e) ice melt date (DOY), (f) the date when ice retreat starts (DOY), (g) the date when ice retreat ends (DOY), and (h) the date when ice advances (DOY), for the southern (black) and northern (gray) model locations. Lines are used when regressions are significant and gray shading represents the 95% confidence interval for these regressions.

3.2. Interannual Changes in Annual NPP

In the south, annual NPP (ice algal + phytoplankton) averaged 109.0 ± 8.9 g C m^{-2} yr^{-1} (Figure 4a) and was 25.8% higher than in the north (Table 3). New production in the south averaged 87.3 ± 8.0 g C m^{-2} yr^{-1}, 28.0% higher than in the north. Different environmental controls drove interannual variability in annual NPP in the northern and southern Chukchi Sea. While ice thickness and the length of the UI period explained much of the variance in annual NPP in the north (Payne et al., 2021), variation in annual NPP in the south was better

Table 3
Average Sea Ice and Snow Conditions and Biogeochemistry at the Northern and Southern Chukchi Sea Model Locations for 1988–2018, With Standard Deviation and p-Values

Variable	North	South	*P*-value
Ice age (yr)	1.5 ± 1.1	0.45 ± 0.05	<0.001
Ice thickness (m)	2.0 ± 0.4	1.5 ± 0.1	<0.001
Snow thickness (cm)	12.9 ± 4.8	8.7 ± 3.1	<0.001
Snow melt date (DOY)	104 ± 30	77 ± 19	<0.001
UI period start (DOY)	137 ± 21	111 ± 10	<0.001
Ice melt date (DOY)	140 ± 11	132 ± 15	0.026
Ice retreat start (DOY)	178 ± 14	138 ± 13	<0.001
Ice retreat end (DOY)	210 ± 22	157 ± 12	<0.001
Ice advance (DOY)	320 ± 20	336 ± 16	<0.001
IA period (d)	31.5 ± 24.8	53.8 ± 21.4	<0.001
UI period (d)	41.8 ± 18.1	27.9 ± 13.6	<0.001
MIZ period (d)	31.3 ± 15.0	18.4 ± 7.6	<0.001
OW period (d)	109.7 ± 38.4	152.3 ± 13.1	<0.001
Annual NPP (g C m^{-2} yr^{-1})	89.0 ± 8.0	109.0 ± 8.9	<0.001
IA NPP (g C m^{-2} yr^{-1})	1.7 ± 1.5	3.0 ± 1.3	<0.001
UI NPP (g C m^{-2} yr^{-1})	44.3 ± 22.6	18.4 ± 17.2	<0.001
MIZ NPP (g C m^{-2} yr^{-1})	20.1 ± 15.6	24.3 ± 16.0	0.3
OW NPP (g C m^{-2} yr^{-1})	22.8 ± 8.0	63.3 ± 11.6	<0.001
Annual Grazing (g C m^{-2} yr^{-1})	7.5 ± 1.4	19.1 ± 2.8	<0.001
UI Grazing (g C m^{-2} yr^{-1})	1.4 ± 0.5	1.2 ± 0.4	0.039
MIZ Grazing (g C m^{-2} yr^{-1})	1.1 ± 0.6	0.5 ± 0.2	<0.001
OW Grazing (g C m^{-2} yr^{-1})	4.9 ± 1.9	17.2 ± 3.0	<0.001
Export to benthos (mmol N m^{-2} yr^{-1})	301.4 ± 44.5	401.9 ± 53.0	<0.001
WC Nitrification (mmol N m^{-2} yr^{-1})	481.5 ± 22.3	573.7 ± 49.3	<0.001
S. Nitrification (mmol N m^{-2} yr^{-1})	186.4 ± 22.2	224.5 ± 16.3	<0.001
S. Denitrification (mmol N m^{-2} yr^{-1})	178.8 ± 28.3	262.4 ± 24.6	<0.001

explained by snow conditions, with years with a longer IA period ($R^2 = 0.382$, $p < 0.001$) or thinner snow ($R^2 = 0.243$, $p = 0.005$) yielding higher NPP.

Interannual variability in southern Chukchi Sea NPP was driven not by NPP during the UI, MIZ, and OW periods, but rather by a reduction in autumn NPP between 1988 and 2018 (Figure 5a). Over this 31 year period, modeled September and October NPP diminished each year by 0.21 g C m^{-2} yr^{-1} ($R^2 = 0.186$, $p = 0.015$) and 0.25 g C m^{-2} yr^{-1} ($R^2 = 0.127$, $p = 0.049$), respectively. The frequency of autumn blooms did not diminish at our model location in the satellite record between 2003 and 2018, where there were no significant changes in NPP. However, due to the low solar angle in the autumn, ocean color data were not available following 21 September each year, making it impossible to evaluate changes in NPP in September and October from the satellite record. However, modeled NPP in September and October was negatively correlated with both the satellite-derived maximum SST ($R^2 = 0.231$, $p = 0.006$ and $R^2 = 0.209$, $p = 0.010$, respectively) and the date when the modeled MLD dropped below 35 m ($R^2 = 0.655$, $p < 0.001$ and $R^2 = 0.153$, $p = 0.030$, respectively). While satellite-derived SST has not changed significantly in September, SST increased by 1.8°C in October ($R^2 = 0.294$, $p = 0.002$) and by 1.6°C in November ($R^2 = 0.275$, $p = 0.002$) between 1988 and 2018. Further, NPP in September and October were both negatively correlated with satellite-derived SSTs during those months ($R^2 = 0.207$, $p = 0.010$ and $R^2 = 0.273$, $p = 0.003$ for September and October, respectively). These correlations indicate that in years when summer SSTs

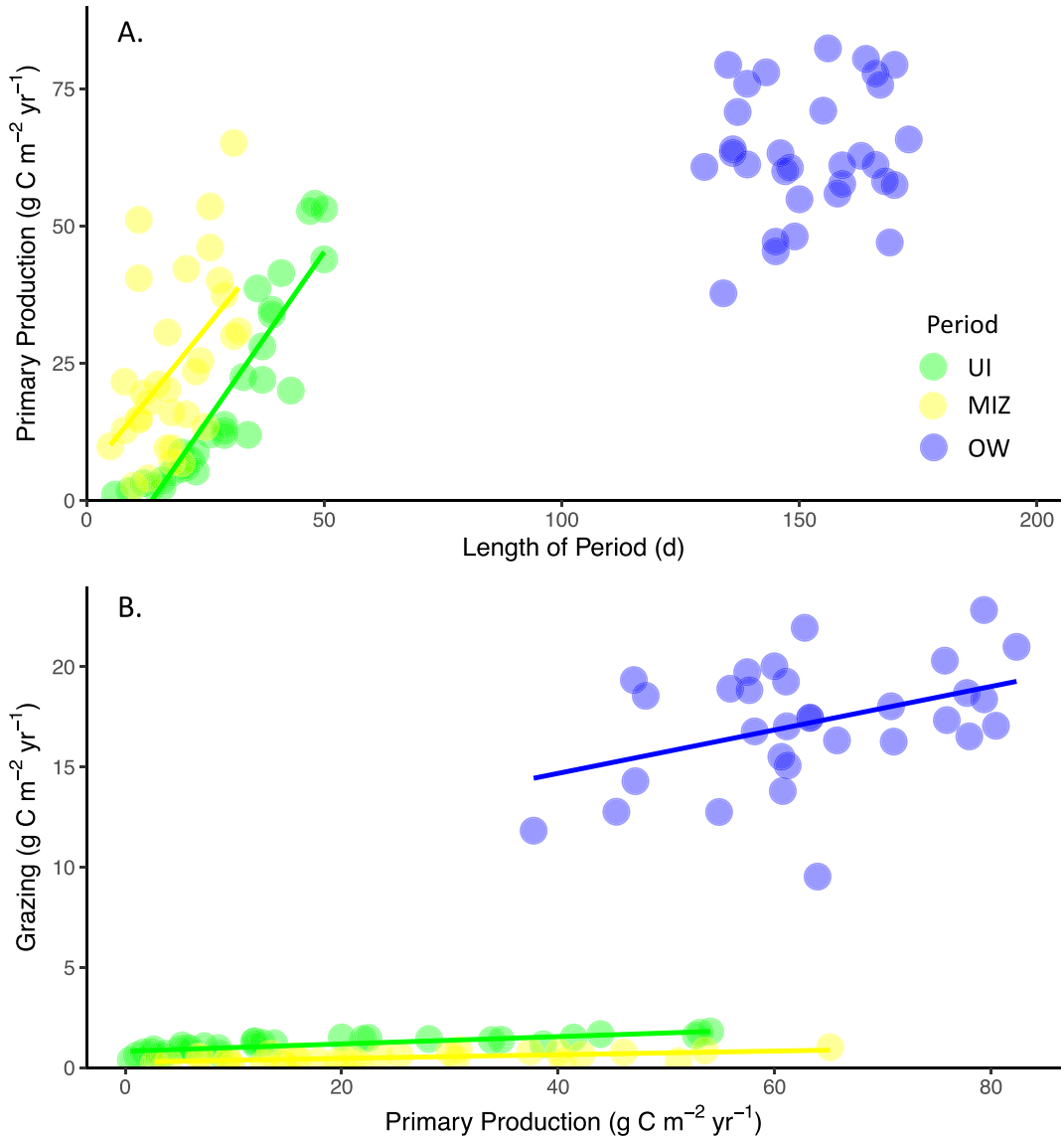

Figure 3. Scatterplots for the southern Chukchi Sea of (a) the length of the period (d) vs. seasonal net primary production (NPP) (g C m^{-2} yr^{-1}) and (b) seasonal NPP vs. seasonal grazing (g C m^{-2} yr^{-1}) for the UI (green), MIZ (yellow), and OW (blue) periods. Lines (in the season color) are used when linear regressions are significant ($p < 0.05$) and gray shading represents the 95% confidence interval for these regressions.

were higher, there was stratification until later in the year, preventing the entrainment of new nutrients in the water column and reducing the incidences of autumn blooms.

3.3. NPP and Zooplankton Grazing in the IA, UI, MIZ, and OW Periods

NPP during the IA period averaged 3.0 ± 1.3 g C m^{-2} yr^{-1} between 1988 and 2018 in the southern Chukchi Sea (Figure 4a), accounting for 2.6% ± 1.0% of annual NPP (Table 5). These annual rates for ice algae were 76.5% higher than those in the northern Chukchi Sea (Table 3). 90.0% of the variance ($p < 0.001$) in annual NPP by ice algae was controlled by the length of the snow melt period ($R^2 = 0.660$, $p < 0.001$), with a longer period of snow melt yielding higher NPP by ice algae.

The UI period accounted for nearly half of annual NPP in the northern Chukchi Sea (Table 3) but a mere 16.3% ± 15.4% of annual NPP in the south (18.4 ± 17.2 g C m^{-2} yr^{-1}; Figure 4b) between 1988 and 2018. While

Table 4
Secular Trends (slope, R^2, and p-value) for the Northern (N.) and Southern (S.) Chukchi Sea in Snow Thickness (cm yr^{-1}), the Dates of Ice Condition Transitions (d yr^{-1}), the Lengths of the UI and OW Periods (d yr^{-1}), Changes in annual and UI NPP (g C m^{-2} yr^{-1}), Changes in Grazing During the UI and OW Periods (g C m^{-2} yr^{-1}), and changes in N Cycle Processes (mmol N m^{-2} yr^{-1})

Variable	N. trend	N. R^2	N. *p*-value	S. trend	S. R^2	S. *p*-value
Snow thickness	−0.24	0.206	0.010	-	-	-
Snow melt date	−1.2	0.139	0.039	-	-	-
UI period start	−1.1	0.231	0.006	-	-	-
Ice retreat start	−0.88	0.327	<0.001	−0.64	0.211	0.009
Ice retreat end	−1.4	0.315	0.001	−0.64	0.219	0.008
Ice advance	1.1	0.244	0.005	0.99	0.367	<0.001
UI period	-	-	-	−0.71	0.221	0.008
OW period	2.5	0.345	<0.001	0.71	0.242	0.005
Annual NPP	0.34	0.148	0.033	-	-	-
UI NPP	-	-	-	−0.80	0.177	0.019
UI grazing	-	-	-	−0.02	0.179	0.018
OW grazing	-	-	-	0.12	0.127	0.050
Export to benthos	1.8	0.130	0.046	-	-	-
WC nitrification	1.2	0.239	0.005	−2.8	0.262	0.003
S. nitrification	1.1	0.220	0.008	−0.7	0.171	0.021
S. denitrification	1.3	0.179	0.018	-	-	-

this period had the highest proportion of new production (89.9% ± 2.9% new production) of any period in the southern Chukchi Sea, it accounted for only 16.3 g C m^{-2} yr^{-1} of total new production, a rate that was lower than both the MIZ and OW periods. Furthermore, NPP in the UI period diminished by 0.8 g C m^{-2} yr^{-1} (Figure 4b and Table 4) between 1988 and 2018. Interannual variance in NPP during the UI period ($R^2 = 0.860$, $p < 0.001$) was controlled primarily by the length of the UI period ($R^2 = 0.798$, $p < 0.001$; Figure 6a), but also by the length of the IA period ($R^2 = 0.062$, $p = 0.002$), with a longer UI period and shorter snow melt period yielding more NPP during the UI period.

NPP in the MIZ period was not significantly different between the north and south (Table 3). In the south, NPP during the MIZ period reached an average of 24.3 ± 16.0 g C m^{-2} yr^{-1} (Figure 4c) and accounted for 21.6% ± 13.5% of annual NPP (Table 5). On average, 77.7% of the annual NPP during the MIZ period was new production, contributing 19.9 ± 13.4 g C m^{-2} yr^{-1} in the southern Chukchi Sea. In the north, NPP transitioned from surface waters to the subsurface chlorophyll maximum (SCM; Payne et al., 2021) during the MIZ period. In contrast, in the south, 87.3% of the NPP during the MIZ period was generated in surface waters. Multiple linear regression revealed that 77.0% of the variance ($p < 0.001$) in NPP during the MIZ period in the southern Chukchi Sea was controlled by the length of the UI period ($R^2 = 0.390$, $p < 0.001$), the length of the MIZ period ($R^2 = 0.224$, $p < 0.001$; Figure 6a), and the length of the IA period ($R^2 = 0.156$, $p < 0.001$). Shorter UI periods and longer MIZ periods yielded more NPP during the MIZ period, while a shorter IA period was correlated with a longer and more productive UI period and thus was associated with reduced NPP during the MIZ period.

Between 1988 and 2018, NPP in the southern Chukchi Sea during the OW period averaged 63.3 ± 11.6 g C m^{-2} yr^{-1} (Figure 4d), nearly three times higher than NPP in the OW period in the north (Table 3). The OW period accounted for most (56.9% ± 11.1%) of the annual NPP in the southern Chukchi Sea (Table 5), and 71.2% of all NPP during the OW period was new production (45.5 ± 9.0 g C m^{-2} yr^{-1}). Most of the NPP during this period (81.2% ± 16.2%) was associated with the SCM. Variation in the length of the OW period was not significantly correlated to the magnitude of NPP during OW period ($p < 0.001$; Figure 6a). 31.0% of the variance ($p = 0.006$) in NPP during the OW period was controlled by snow thickness ($R^2 = 0.167$, $p = 0.014$) and the length of the MIZ period ($R^2 = 0.143$, $p = 0.022$). Due to the very long OW period (152.3 ± 13.1 d), NPP was not correlated with the length of the OW period in the southern Chukchi (Figure 6a) and was instead greatest when thick snow prevented NPP during the UI period and a short MIZ period prevented NPP during the MIZ period.

Zooplankton grazed phytoplankton at an average rate of 19.1 ± 2.8 g C m^{-2} yr^{-1} between 1988 and 2018 (17.2% ± 2.9% of annual NPP), 1.5 times greater than in the north (Table 3). During the UI period, grazing by zooplankton in the southern Chukchi Sea averaged 1.2 ± 0.4 g C m^{-2} yr^{-1}, consuming 15.8% ± 16.7% of NPP in the UI period. Zooplankton grazing during the MIZ period in the south averaged 0.5 ± 0.2 g C m^{-2} yr^{-1} (0.4% ± 0.2% of NPP in the MIZ period) or less than half of the grazing during the MIZ period in the north. Southern Chukchi Sea zooplankton consumed 17.2 ± 3.0 g C m^{-2} yr^{-1} during the OW period (or 27.7% ± 5.6% of OW period NPP), 2.5 times more biomass than was typically consumed in the north (Table 3). While southern Chukchi Sea grazing diminished by 0.02 g C m^{-2} yr^{-1} yr^{-1} during the UI period ($R^2 = 0.179$, $p = 0.018$), grazing increased by 0.12 g C m^{-2} yr^{-1} in the OW period ($R^2 = 0.127$, $p = 0.050$). NPP during the UI, MIZ, and OW periods was significantly correlated with grazing during that period (Figure 6b).

3.4. PON Export to the Benthos

The amount of PON exported to the benthos averaged 401.9 ± 53.0 mmol N m^{-2} yr^{-1} in the southern Chukchi Sea, a rate 33.3% higher than the rate in the north (Table 3). 33.0% ± 1.7% of the annual N assimilated by microalgae (and 42.7% ± 3.1% of the total annual NO_3^- assimilation by microalgae) was exported to the benthos.

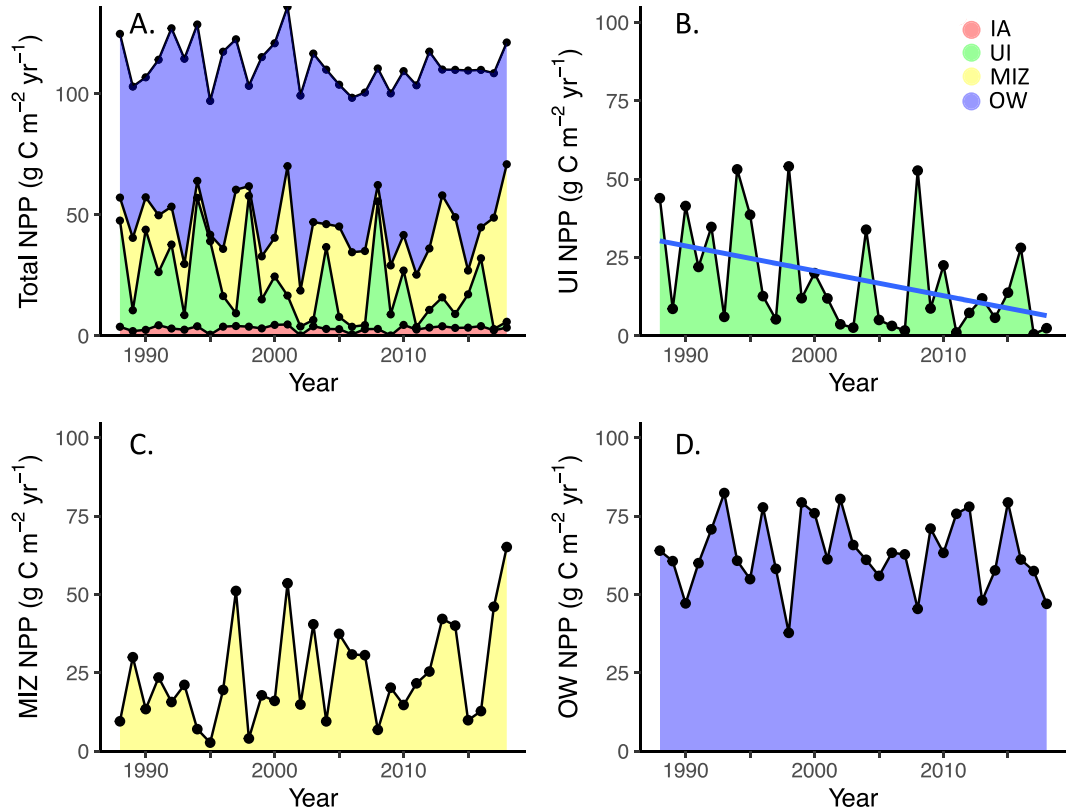

Figure 4. (a) Annual net primary production (NPP; upper black line) in the southern Chukchi Sea and its component parts, ice algal (IA) NPP (red), (b) annual UI NPP (green), (c) annual MIZ NPP (yellow), and (d) annual OW NPP (blue) between 1988 and 2018. A blue line is used to indicate the statistically significant decline in UI NPP.

Daily PON export peaked on average at 5.2 ± 1.5 mmol N m^{-2} d^{-1} (Figure 7a). As in Payne and Arrigo (2022), PON export to the sediments was highly correlated with annual N assimilation by microalgae, which in the south explained 97.4% of the variance in PON export ($p < 0.001$). In addition, interannual variance in PON export could be explained by snow thickness ($R^2 = 0.242$, $p = 0.005$) and the length of the snow melt period ($R^2 = 0.239$, $p = 0.005$), the primary drivers of variance in annual NPP. Between 1988 and 2018, PON export increased marginally in August but diminished in September and October (Table 6 and Figure 7a) due to the reduction in N assimilated by microalgae during the autumn.

3.5. Nitrification and Denitrification

Between 1988 and 2018, daily depth-integrated water column nitrification rates in the south ranged from 0.01 ± 0.004 to 8.9 ± 1.3 mmol N m^{-2} d^{-1} (Figure 7b), peaking in early June (on DOY 155.4 ± 12.5). Annual nitrification rates averaged 573.7 ± 49.3 mmol N m^{-2} yr^{-1} in the southern Chukchi Sea, equivalent to 46.1% ± 3.3% of annual N assimilation by microalgae. These annual water column nitrification rates diminished by 2.8 mmol N m^{-2} yr^{-1} ($R^2 = 0.262$, $p = 0.003$) between 1988 and 2018 but were still 19.1% higher than rates to the north (Table 3). 72.2% of the variance ($p < 0.001$) in annual water column nitrification was controlled by the length of the OW ($R^2 = 0.468$, $p < 0.001$) and UI periods ($R^2 = 0.254$, $p = 0.025$). Furthermore, changes in annual N assimilation by microalgae explained 40.0% of the interannual variance in water column nitrification ($p < 0.001$). Variation in N assimilation during the UI period accounted for 30.5% of the variance in water column nitrification ($p = 0.001$), more than N assimilation in the IA ($R^2 = 0.167$, $p = 0.023$), MIZ ($R^2 = 0.135$, $p = 0.042$), or OW (no statistically significant relationship) periods. Decreases in annual water column nitrification in the southern Chukchi Sea between 1988 and 2018 were driven by decreases during January, February, September, and October (Figure 7b and Table 6) due to lowered incidences of autumn blooms.

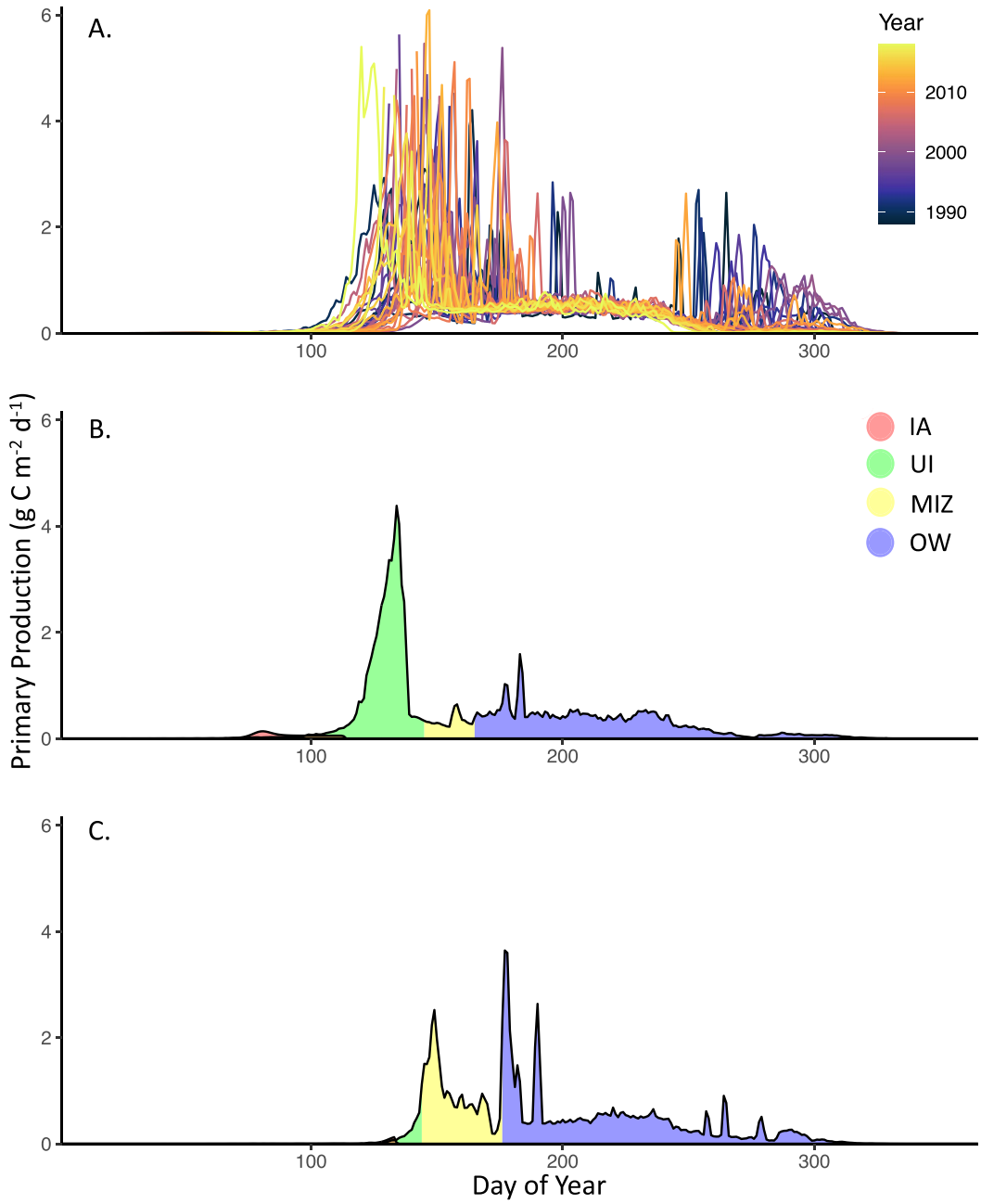

Figure 5. (a) Daily water-column net primary production (NPP) for 1988–2018 in the southern Chukchi Sea, and example annual cycles of daily NPP (g C m^{-2} d^{-1}) for (b) a year with a UIB (2008), and (c) a year without a UIB (2006). Red shading represents production by ice algae while green, yellow, and blue shading represent production during UI, MIZ, and OW periods, respectively.

Daily sedimentary nitrification rates in the southern Chukchi Sea ranged from 0.29 ± 0.05 to 1.0 ± 0.04 mmol m^{-2} d^{-1} (Figure 7c) between 1988 and 2018. Annual rates were substantially lower than rates in the water column, averaging 224.5 ± 16.3 mmol N m^{-2} yr^{-1} and were 20.4% higher than corresponding rates in the north (Table 3). Nitrification in the sediments accounted for an average of 18.5% ± 1.2% of annual N assimilated by microalgae in the southern Chukchi Sea and 56.4% ± 5.3% of the exported PON. Rates of sedimentary nitrification diminished by 0.7 mmol N m^{-2} yr^{-1} each year between 1988 and 2018 ($R^2 = 0.171$, $p = 0.021$). The variability in annual sedimentary nitrification was controlled primarily by the amount of N assimilated by microalgae ($R^2 = 0.481$, $p < 0.001$) and subsequently exported to the benthos ($R^2 = 0.503$, $p < 0.001$). Sedimentary nitrification vari-

Table 5
Bloom Type, % IA, % UI, % MIZ, % OW, and Annual NPP (g C m^{-2} yr^{-1}) for Each Year in the Southern Chukchi Sea

Year	Bloom type	% IA	% UI	% MIZ	% OW	Annual
1988	UIB	3.1	36.3	7.8	52.8	121.1
1989	N	1.9	7.1	24.7	50.1	101.1
1990	UIB	2.4	34.2	11.1	38.9	104.4
1991	N	4.0	18.1	19.4	49.5	109.8
1992	UIB	2.4	28.7	12.9	58.4	124.2
1993	N	2.3	5.0	17.4	68.0	112.0
1994	UIB	3.2	43.9	5.8	50.2	124.8
1995	UIB	0.5	31.9	2.2	45.3	96.7
1996	N	3.3	10.5	16.1	64.2	113.7
1997	N	3.4	4.3	42.2	48.0	118.6
1998	UIB	3.8	44.6	3.3	31.2	99.6
1999	N	2.7	9.9	14.7	65.5	112.2
2000	N	3.9	16.5	13.2	62.7	116.4
2001	N	3.6	9.8	44.2	50.5	131.4
2002	N	0.2	3.0	12.3	66.4	99.1
2003	N	3.5	2.2	33.4	54.3	112.8
2004	UIB	2.6	28.0	7.8	50.4	107.2
2005	N	2.7	4.2	30.9	46.2	101.1
2006	N	0.6	2.6	25.5	52.3	97.8
2007	N	2.8	1.4	25.3	51.8	97.8
2008	UIB	2.6	43.5	5.6	37.5	107.7
2009	N	0.1	7.2	16.7	58.6	100.1
2010	UIB	4.3	18.6	12.1	52.2	104.9
2011	N	2.6	0.9	17.8	62.5	101.0
2012	N	3.0	6.0	21.0	64.4	114.1
2013	N	3.7	9.9	34.8	39.7	106.1
2014	N	3.0	4.8	33.1	47.6	106.7
2015	N	3.2	11.4	8.1	65.5	106.3
2016	UIB	3.8	23.2	10.5	50.5	105.9
2017	N	2.1	0.4	38.0	47.4	106.3
2018	N	2.9	2.0	53.8	38.8	117.9
Mean	UIB	2.9 ± 1.1	36.9 ± 10.3	8.7 ± 4.0	51.5 ± 7.7	109.6 ± 10.1
Mean	N	2.6 ± 1.1	7.2 ± 5.3	28.6 ± 12.3	61.6 ± 11.2	108.7 ± 8.5

Note. Annual cycles of NPP were separated into two clusters (bloom types): years with UIBs (UIB) and years without UIBs (N). Means and standard deviation of annual NPP (g C m^{-2} yr^{-1}) and NPP within the UI, MIZ, and open water (OW) periods (%) for both of the clusters are listed at the bottom of the table.

ance was best explained by snow thickness ($R^2 = 0.242$, $p = 0.005$), the primary driver of variance in both annual N assimilation by microalgae and PON export to the benthos. Decreases in annual sedimentary nitrification between 1988 and 2018 were driven by decreases in nitrification rates in January–April and September–December (Figure 7c and Table 6) caused by the reduction in PON exported to the benthos in the autumn.

Because of relatively high concentrations of O_2 in the water column, our model configuration produces no denitrification in the water column. However, modeled sedimentary denitrification rates in the south could be substantial, ranging from 0.26 ± 0.04 to 1.5 ± 0.2 mmol N m^{-2} d^{-1} (Figure 7d). Annual denitrification rates were

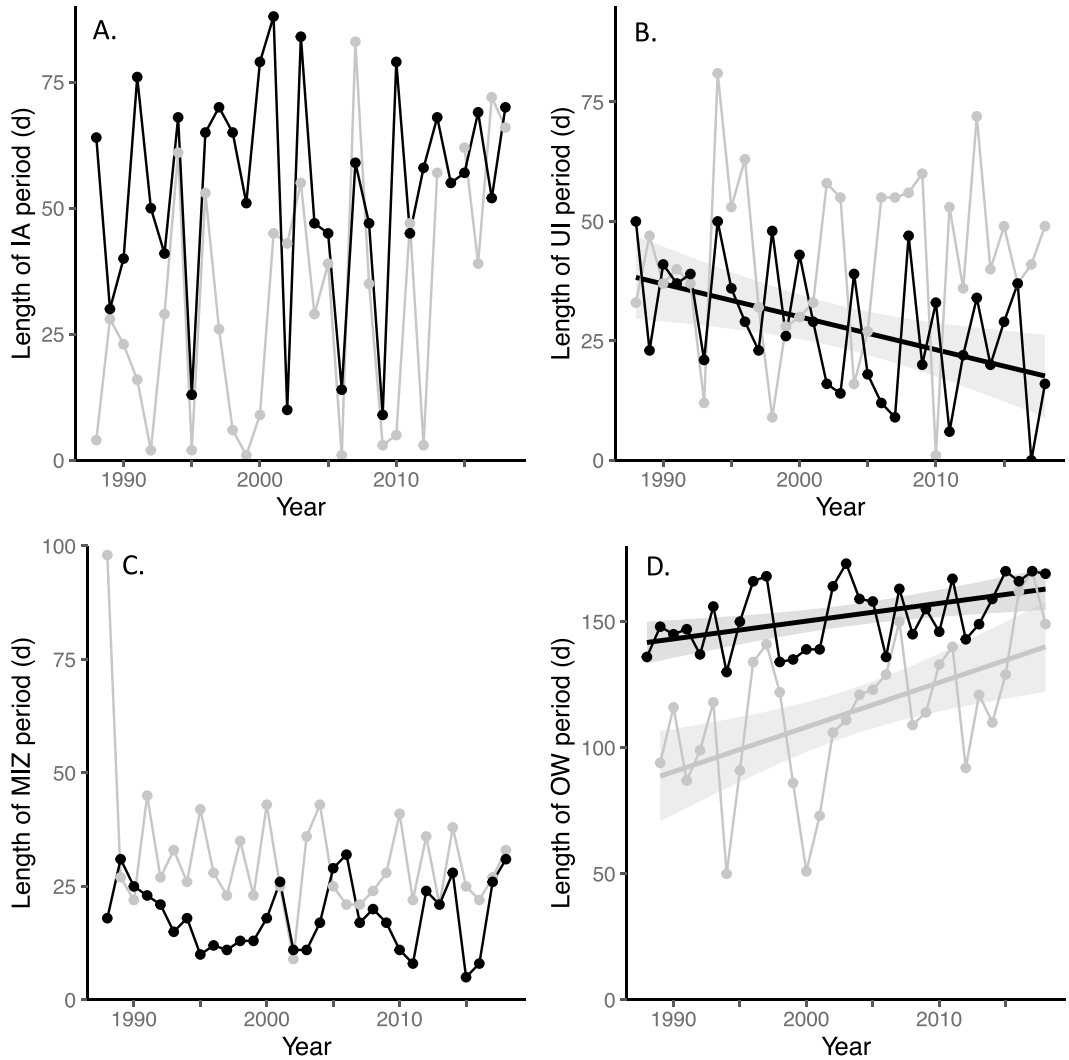

Figure 6. Lengths between 1988 and 2018 of the (a) IA period (d), (b) UI period (d), (c) MIZ period (d), and (d) OW period (d), for the southern (black) and northern (gray) model locations. Lines are used when linear regressions are statistically significant and gray shading represents the 95% confidence interval for these regressions.

46.8% higher than those to the north (Table 3), averaging 262.4 ± 24.6 mmol N m^{-2} yr^{-1} between 1988 and 2018, and did not change significantly over time. Sedimentary denitrification in the southern Chukchi Sea removed 21.6% ± 1.2% of the annual N assimilated by microalgae, 65.7% ± 4.6% of the PON exported to the sediments, and 116.8% ± 4.3% of the NO_3^- produced through sedimentary nitrification. Denitrification was closely correlated with N assimilation by microalgae ($R^2 = 0.668$, $p < 0.001$) and PON export to the benthos ($R^2 = 0.743$, $p < 0.001$), and thus shared the same environmental drivers of interannual variability (snow thickness, with $R^2 = 0.239$ and $p = 0.005$, and the length of the snow melt period, with $R^2 = 0.140$ and $p = 0.038$). Annual sedimentary denitrification showed no trend over time, but sedimentary denitrification diminished in January–April and October–December and increased in August (Figure 7d and Table 6), driven by changes in PON export and sedimentary nitrification due to a reduction in autumn bloom incidence.

In addition to an increase in sedimentary nitrification and denitrification in the southern Chukchi Sea relative to the north, there was a difference in the balance between the two processes. In the north, 62% and 59% of the PON exported to the benthos was subsequently nitrified and denitrified, respectively. As a result, there was slightly more nitrification than denitrification in the sediments (7.6 mmol m^{-2} yr^{-1} more; Table 3). However, in the south, only 56% of the PON exported to the benthos was nitrified, but the relative amount of exported PON that was denitrified increased to 65%. This shifted the balance between sedimentary nitrification and denitrification to

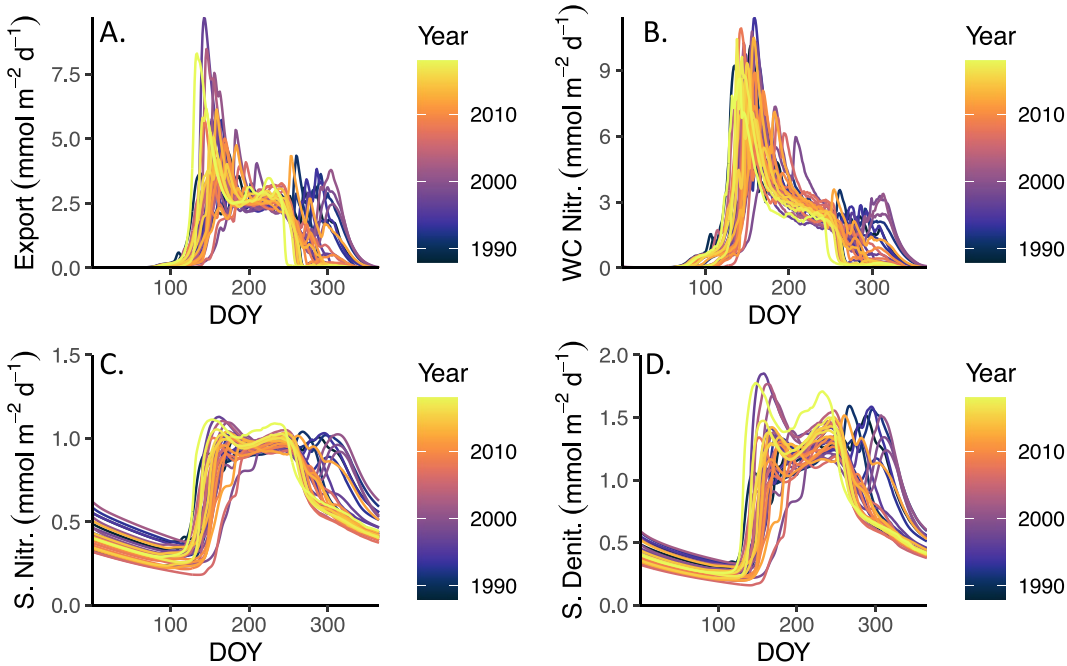

Figure 7. Rates of (a) PON export to the benthos (mmol N m^{-2} d^{-1}), (b) water column nitrification (WC Nitr., mmol N m^{-2} d^{-1}), (c) sedimentary nitrification (S. Nitr., mmol N m^{-2} d^{-1}), and (d) sedimentary denitrification (S. Denit., mmol N m^{-2} d^{-1}) for each day of the year (DOY) between 1988 and 2018 (colorbar) in the southern Chukchi Sea.

favor denitrification, which on average removed 37.9 mmol N m^{-2} yr^{-1} more than was converted to NO_3^- through sedimentary nitrification (Table 3). As a result, denitrification in the southern Chukchi Sea relied on more NO_3^- that had diffused across the sediment-water interface as substrate. The balance between nitrification and denitrification was controlled ($R^2 = 0.969$, $p < 0.001$) by the location ($R^2 = 0.515$, $p < 0.001$) and the amount of PON exported to the benthos ($R^2 = 0.454$, $p < 0.001$; Figure 8a). The differences between the north and south arose because of differences in phenology, with the amount of N assimilation during the OW period controlling more of the variance in the nitrification-denitrification balance ($R^2 = 0.760$, $p < 0.001$; Figure 8b) than any other metrics of phenology (lengths of the period of production and N assimilation during each period). The rate of PON export to the benthos controlled the balance of nitrification and denitrification because it drove higher oxygen utilization in the surface layers sediments. In the south, the higher rates of PON export to the benthos corresponded to a far thinner oxic layer, allowing denitrification higher in the sediments (mean depth of 5 mm between June and November) than to the north (mean depth of 9 mm).

3.6. Water Column Bloom Types

In order to characterize patterns of bloom evolution in the southern Chukchi Sea, we performed clustering analysis that categorized years based on NPP during the UI and MIZ periods. In the north, this resulted in three different types of annual cycles: 17 years dominated by NPP in the UI period (where NPP in the UI period accounted for a mean of 65.0% ± 7.6% of annual NPP), four MIZ-dominant years (where NPP in the MIZ period averaged 64.5% ± 2.7% of annual NPP), and 10 mixed-dominance years (where NPP during the UI and MIZ periods averaged 39.5% ± 9.7% and 30.1% ± 7.8% of annual NPP, respectively; Payne et al., 2021). In the south, only two distinct annual cycles were produced through our analysis (Table 5). Because OW blooms dominated annual NPP every year, the major distinguishing feature between years was whether a UIB was present (10 of 31 yr; Figure 5b and Figures S4a, S4c, and S4e in Supporting Information S1) or absent (21 of 31 yr; Figure 5c and Figures S4b, S4d, and S4f in Supporting Information S1). The years with UIBs had nearly five times more NPP in the UI period but less NPP in the MIZ (30.7% of non-UIB years) and OW periods (85.0% of non-UIB years; Table 7). Years that were categorized as having UIBs also had lower peak rates of NPP, less annual zooplankton grazing, and 7.2% higher annual water-column nitrification rates than years without UIBs. There were no significant

Table 6
Linear Regressions (R^2, p-value, and slope) for statistically significant ($p < 0.05$) Changes in Southern Chukchi Sea Monthly Benthic PON Export (mmol N m^{-2} Per Month), Water Column Nitrification (mmol N m^{-2} Per Month), Sedimentary Nitrification (mmol N m^{-2} Per Month), and Sedimentary Denitrification (mmol N m^{-2} Per Month) between 1988 and 2018

Process	Month	R^2	*P*-value	Slope
Benthic export	August	0.158	0.027	1.11E-2
Benthic export	September	0.223	0.007	−2.79E-2
Benthic export	October	0.210	0.009	−4.52E-2
Water column nitrification	January	0.137	0.040	−2.68E-4
Water column nitrification	February	0.227	0.007	−2.28E-4
Water column nitrification	September	0.214	0.009	−2.44E-2
Water column nitrification	October	0.213	0.009	−3.52E-2
Sedimentary nitrification	January	0.144	0.035	−2.95E-3
Sedimentary nitrification	February	0.143	0.036	−2.61E-3
Sedimentary nitrification	March	0.145	0.035	−2.35E-3
Sedimentary nitrification	April	0.159	0.026	−2.22E-3
Sedimentary nitrification	September	0.188	0.015	−1.44E-3
Sedimentary nitrification	October	0.265	0.003	−7.49E-3
Sedimentary nitrification	November	0.156	0.038	−6.98E-3
Sedimentary nitrification	December	0.160	0.026	−3.96E-3
Sedimentary denitrification	January	0.139	0.039	−2.62E-3
Sedimentary denitrification	February	0.147	0.033	−2.29E-3
Sedimentary denitrification	March	0.151	0.031	−2.05E-3
Sedimentary denitrification	April	0.164	0.024	−1.95E-3
Sedimentary denitrification	August	0.141	0.038	2.31E−3
Sedimentary denitrification	October	0.260	0.003	−1.35E-2
Sedimentary denitrification	November	0.144	0.035	−1.04E-2
Sedimentary denitrification	December	0.137	0.040	−3.97E-3

differences in annual NPP, IA NPP, PON export to the benthos, sedimentary nitrification, or sedimentary denitrification between the two bloom patterns.

Environmental conditions determined whether a UIB was generated each year. While ice thickness did not significantly vary between the two bloom types, years with UIBs had thinner snow cover than years without UIBs (Table 7). Years characterized by moderate UIBs also had UI periods that ran nearly twice as long as years without UIBs, although the lengths of other periods (IA, MIZ, and OW periods) were not significantly different.

4. Discussion

4.1. Ice Conditions and Primary Production

The southern Chukchi Sea, long observed to be dominated by thin first-year ice, is currently experiencing a 5 months long ice-free period, a condition that is not expected in the northern Chukchi Sea until 2040 (Wang & Overland, 2015). At present, sea ice retreats in the southern Chukchi Sea more than 1 month earlier and advances 2 weeks later than in the northern Chukchi Sea (Serreze et al., 2016). While the resulting north-south gradient in sea ice concentration is certainly in part a function of latitudinal differences in solar forcing and air temperature, it is also driven by the increasing amount of heat transported through the Bering Strait (Serreze et al., 2016; Shimada et al., 2006; Woodgate, 2018; Woodgate et al., 2012). Across the Chukchi Sea, 67% of the variance in the timing of both ice retreat and advance between 1979 and 2014 was explained by the amount of heat advected through the Bering Strait (Serreze et al., 2016). These heat fluxes through the Bering Strait have increased substantially since the 1990s, driven by a 0.01 Sv yr^{-1} increase in the transport of Pacific waters into the Arctic Ocean (Woodgate, 2018; Woodgate et al., 2012). Differences between the northern and southern Chukchi Sea in the timing of sea ice advance and retreat are projected by CMIP models to extend through at least 2090, with the north remaining ice-covered two months longer than our model location in the south (Wang & Overland, 2015).

The differences in the timing of sea ice loss between the north and the south result in distinctly different growing conditions for sea ice microalgae and phytoplankton in the Chukchi Sea. The earliest source of NPP each year is sea ice microalgae (Arrigo et al., 2017; Fortier et al., 2002). As light increases in the late winter and early spring, microalgae suspended in the bottom 5–10 cm of the sea ice are primed to take advantage of the high water-column NO_3^- concentrations (Arrigo, 2017; Bradstreet & Cross, 1982; Fortier et al., 2002; Gradinger, 1996). IA blooms can be generated more than 1 month earlier than water column blooms (Payne et al., 2021) and provide a critical early burst of NPP to a pelagic ecosystem lacking in food sources (Arrigo et al., 2017; Assmy et al., 2013; Bradstreet & Cross, 1982; Fortier et al., 2002; Gradinger, 2009; Søreide et al., 2010). IA NPP in our study averaged 3.0 g C m^{-2} yr^{-1} in the southern Chukchi Sea, in line with rates observed on other shallow Arctic continental shelves (Arrigo, 2017; Dupont, 2012; Gosselin et al., 1997; Gradinger, 2009; Jin et al., 2012). Further, this rate was significantly higher than in the north, driven by a 3-week longer growing season.

As melt ponds form on the surface of sea ice in the Chukchi Sea, UI phytoplankton blooms can form a second pulse of NPP. Although the sea ice-covered period has historically been considered to be too light-limited to allow for significant phytoplankton growth (Hameedi, 1978; Perrette et al., 2011), observations of massive UI phytoplankton blooms in the Chukchi Sea (Arrigo et al., 2012, 2014; Hill, Light, et al., 2018; Lowry et al., 2014) demonstrated that this period can contribute substantially to annual NPP. It has been estimated that, due to an inability to observe UIBs, satellite-derived NPP is underestimated by more than an order of magnitude in the northern Chukchi Sea (Arrigo et al., 2014; Arrigo & Van Dijken, 2011). In situ observations of UIBs have demonstrated that this period can account for more than half of total NPP (Arrigo et al., 2014; Lowry et al., 2014;

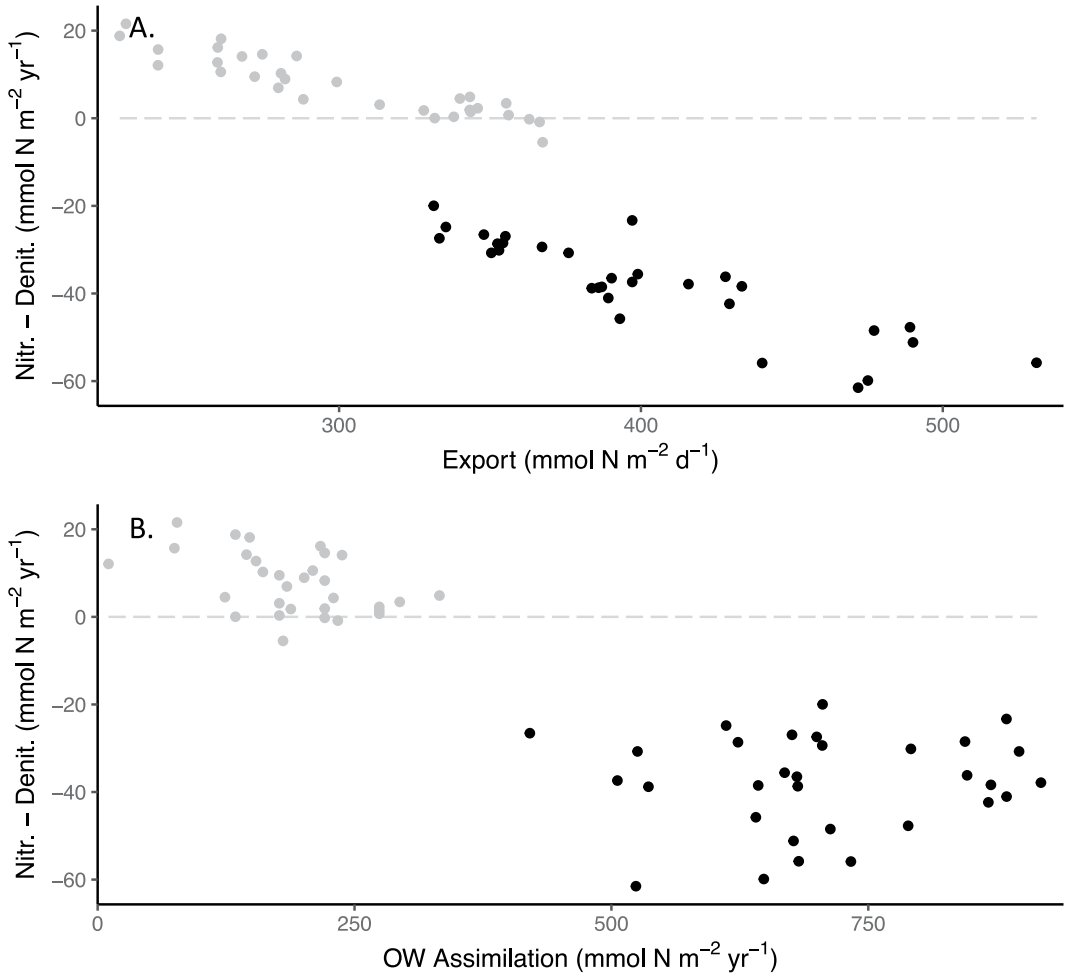

Figure 8. Scatterplots comparing the balance between nitrification and denitrification (mmol N m^{-2} yr^{-1}) to (a) PON export (mmol m^{-2} yr^{-1}) and (b) OW assimilation (mmol N m^{-2} yr^{-1}) for the northern (gray) and southern (black) Chukchi Sea.

Mayot et al., 2018; Mundy et al., 2009; Oziel et al., 2019), and modeling work by Payne et al. (2021) showed that in the north, the UI period accounted for nearly half of annual NPP and drove most of the interannual variability. However, the massive UIBs that can be supported in the northern Chukchi Sea appear in other modeling studies to not be reproduced uniformly across the Chukchi Sea. Zhang et al. (2015) found that while 46% of

Table 7
Differences in Environmental Drivers and Consequences of Water Column Bloom Pattern in the Southern Chukchi Sea

Variable	UIB years	Non-UIB years	*P*-value
Snow thickness (cm)	6.9 ± 2.6	9.6 ± 3.0	0.023
UI period (d)	42.0 ± 6.2	21.1 ± 10.7	<0.001
UI NPP (g C m^{-2} yr^{-1})	44.3 ± 22.6	7.8 ± 6.0	<0.001
MIZ NPP (g C m^{-2} yr^{-1})	9.6 ± 4.5	31.3 ± 14.6	<0.001
OW NPP (g C m^{-2} yr^{-1})	56.6 ± 10.2	66.6 ± 11.0	0.023
Peak daily NPP (g C m^{-2} d^{-1})	3.9 ± 0.6	6.0 ± 2.7	0.021
Annual grazing (g C m^{-2} yr^{-1})	16.9 ± 3.1	20.2 ± 2.0	<0.001
WC nitrification (mmol N m^{-2} yr^{-1})	601.2 ± 47.2	560.6 ± 45.7	0.029

Note. Averages (and standard deviations) are listed for years with and without UIBs, as well as *p*-values.

the Chukchi Sea supported UIBs between 1988 and 2013, massive UIBs covered only 8% of the area over the same period, and that these blooms were largely concentrated in the northern Chukchi Sea near the shelf break. Results from our southern location indicate that the earlier start of sea ice retreat and shorter UI period caused the UI period to only contribute 16% toward annual NPP, supporting the broader trend that Zhang et al. (2015) modeled across the Chukchi Sea. As a result, NPP during the MIZ and OW periods was higher and annual NPP estimated by CAOS-GO was more in line with satellite-derived (MODIS) estimates than in the north (with mean satellite-derived and modeled 2003–2018 NPP of 110.1 ± 35.1 and 105.9 ± 5.6 g C m^{-2} yr^{-1}, respectively; Figure S3 in Supporting Information S1, Lewis & Arrigo, 2020; Lewis et al., 2020).

Furthermore, we found that the contributions of the UI period to annual NPP was reduced by more than 20 g C m^{-2} between 1988 and 2018 in the southern Chukchi Sea, dropping in the last 5 yr of our record to an average of 34% the annual NPP estimated in the first 5 yr. A satellite-based analysis of the prevalence of UIBs and MIZ blooms throughout the Chukchi Sea similarly revealed that the area that likely supported UIBs shrunk between 1998 and 2012 (Lowry et al., 2014), indicating that the shelf region as a whole may be seeing a reduction in the prevalence of UIBs over time. As the Chukchi Sea is predicted to experience a continued decrease in sea ice coverage (Wang & Overland, 2015) and loss of multiyear ice (Serreze et al., 2016; Serreze & Stroeve, 2015), the decreasing trend modeled here indicates that although UIBs contribute substantially to annual NPP in the northern Chukchi Sea (Arrigo et al., 2012, 2014), these blooms may diminish in importance in the future. Model intercomparison work by Jin et al. (2016) indicates this may be an Arctic-wide trend. While all three models in their study found that an increase in open-water area is driving an Arctic-wide increase in NPP, the importance of UIBs differed spatially, with NPP during the UI period increasing in some regions due to the increase in light transmission into the ocean but diminishing in regions with high rates of sea ice loss.

The MIZ period has long been considered to be responsible for the highest rates of NPP and the largest contributor to annual NPP in Arctic waters (Niebauer, 1991; Perrette et al., 2011; Sakshaug, 2004). However, our results suggest that this was not the case in the northern Chukchi Sea, where the MIZ contributed less to annual NPP than both the UI and OW periods because of both nutrient depletion in surface waters during the UI period and the short length of the MIZ period (Payne et al., 2021). While the southern Chukchi Sea had an MIZ period that was, on average, 40% shorter than in the north, NPP during the MIZ period was not significantly different between the two regions. Instead, low NO_3^- utilization during the UI period in the south allowed for substantially higher rates of NPP in surface waters during the MIZ period. While there are no known in situ measurements of NPP during the MIZ period near the southern model location, observations at the beginning of the OW period during ICESCAPE 2011 indicate that phytoplankton biomass and NPP were highest in the top 20 m of the water column (Arrigo et al., 2014). Similarly, several remote sensing studies (Lowry et al., 2014; Perrette et al., 2011) have observed MIZ blooms at our southern model location, indicating that NPP increased in the mixed layer following sea ice retreat. These observations, paired with our model results, indicate that the loss of sea ice in the early spring allows the MIZ period to contribute a disproportionate 22% toward annual NPP relative to its short duration (18 days) in the southern Chukchi Sea.

Because NPP during the UI and MIZ periods consumes most of the nutrients in the surface waters of the Chukchi Sea, NPP during the OW period is dominated by phytoplankton growing in a SCM (Arrigo et al., 2014; Brown et al., 2015; Hill & Cota, 2005; Martin et al., 2010). As the OW period throughout the Chukchi Sea has increased (by 37 days between 1998 and 2018), satellite-derived estimates of NPP in the Chukchi Sea have nearly doubled (Lewis et al., 2020). While NPP during the OW period contributed minimally to total NPP (26%) in the northern Chukchi Sea, it generated more than half of the annual NPP in the south. The far larger OW blooms in the southern Chukchi Sea are expected to support much larger zooplankton populations than in the north. In both locations, zooplankton grazed more during the warmer waters of the OW period when growth was less constrained by cold temperatures (Campbell et al., 2001; Huntley & Lopez, 1992; Payne et al., 2021). However, the far higher rates of annual grazing in the south and the increase in grazing over time indicate that the longer OW period and higher SSTs in the south (Richter-Menge et al., 2019) might allow for richer pelagic ecosystems than in the northern location.

Although our model did not produce a change in NPP during the OW period at either location between 1988 and 2018, there was a 14.3 g C m^{-2} yr^{-1} decrease in NPP during September and October in the southern Chukchi Sea. Remote sensing studies of the Arctic Ocean (Ardyna et al., 2014) and of the Chukchi and Bering Seas (Waga & Hirawake, 2020) indicate that autumn blooms have increased in many sectors of the Arctic Ocean, including in

the southern Chukchi Sea, between 1998 and 2017. However, these studies also demonstrate the patchy nature of autumn blooms, and both studies find a low incidence of autumn blooms at our model location. Our model results suggest that the lack of autumn blooms in some parts of the southern Chukchi Sea may be attributable to a greater degree of stratification than at similar latitudes in the Arctic. We found that, as SSTs increased over time at our southern location (Osborne et al., 2018), rising to 11°C by 2018, the water column remained stratified until later in the year. This finding is supported by satellite observations—at our model location in the southern Chukchi Sea, SSTs have increased by an average of 1.7°C in both October and November. Our model results indicate that this increased stratification could prevent the entrainment of deep NO_3^- into the upper water column in the autumn (see the depth vs. time plots for a year with and without an autumn bloom in Figures S4a–S4d in Supporting Information S1) and prevent the formation of autumn phytoplankton blooms. Due to the patchy nature of fall blooms, these model results may not be representative of the entire Chukchi shelf. However, they highlight that increasing SSTs may prevent mixing in the fall and may lead to a reduction in incidences of autumn blooms as the Arctic warms further in the future.

4.2. Particulate Export and Fixed N Loss

Because of the shallow continental shelf and high rates of NPP in the Chukchi Sea, particle export to the benthos can be substantial. In the northern Chukchi Sea, CAOS-GO produced an average POC export rate of 29.2 ± 4.3 g C m^{-2} yr^{-1} between 1988 and 2018, similar to the Chukchi Sea-wide estimate of 29.7 g C m^{-2} yr^{-1} (Chang & Devol, 2009). Similarly, Chl *a* export rates derived from moorings deployed above the seafloor by Lalande et al. (2020) Nishino et al. (2016) compare favorably with modeled Chl *a* export rates to the benthos. For instance, in the northern Chukchi Sea, a mooring deployed at 37 m depth (8 m above the seafloor) observed a mean export rate of 3–5 mg Chl *a* m^{-2} d^{-1} during a UIB in June–July 2016, while CAOS-GO produced an export rate of 3–4.8 mg Chl *a* m^{-2} d^{-1} during this same period. In the southern Chukchi Sea, a mooring deployed by Nishino et al. (2016) between 2012 and 2014 captured a sudden increase in exported Chl *a* during the UI period in mid-May of 2013, peaking in mid-June, remaining high (1–15 mg Chl *a* m^{-3}) until mid-July, and finally dropping below 1 mg Chl *a* m^{-3} in mid-October. Similarly, CAOS-GO found that, at a depth of 45 m, Chl *a* began to rapidly increase on 15 May and peaked on 9 June 2013. Following a bloom of 3 weeks, Chl *a* remained elevated until the beginning of July, when it diminished to around 1 mg Chl *a* until late September, when Chl *a* concentrations started to drop. While the phenology of exported Chl *a* between the mooring and our model are in good agreement, the magnitude of the bloom observed by the fluorometer on the Nishino et al. (2016) mooring near the end of its 10 months long deployment was substantially larger, reaching as high as 30 mg Chl *a* m^{-3}.

The amount of NPP produced during the four distinct microalgal bloom periods has important consequences on the regional N cycle of the Chukchi Sea. High rates of NPP provide more biomass for export to the benthos, which on the Chukchi shelf is associated with a loss of fixed N through coupled partial nitrification-denitrification (Brown et al., 2015). The Chukchi Sea accounts for a disproportionately large amount of global N loss in the oceans as a result of its high export production and shallow continental shelf (Chang & Devol, 2009). While observational studies have yet to compare denitrification rates near our model locations, limited in situ observations indicate that sedimentary oxygen utilization in the south is twice as high as in north (Granger et al., 2018; Grebmeier, 2012; Reeve et al., 2019), which is evidence of enhanced supply of C and N to the benthos and higher denitrification in the south. Consistent with these observations, we found that the south featured higher rates of PON export to the benthos than the north, contributing to a nearly 50% higher loss of fixed N through denitrification in the south. Further, we found that denitrification outweighed nitrification in the sediments of the southern Chukchi Sea. Our model found that the balance between nitrification and denitrification was controlled by the phenology of NPP and the rate of PON export to the benthos, with years with more NPP later in the year and higher total PON export seeing more denitrification than nitrification. While no studies that we are aware of have captured the annually integrated balance between sedimentary nitrification and denitrification, this finding highlights that, because denitrification can use NO_3^- diffused across the sediment-water boundary, denitrification rates can exceed the supply of NO_3^- produced locally in the sediments through nitrification.

More importantly, our results demonstrate that the drivers of interannual variation in the N cycle differ substantially between the northern and the southern Chukchi Sea. In the north, the UI period dominated annual production in most years (17 of 31), with an average of 65% of annual NPP generated during the UI period in those years. UI-dominated years had 16% higher annual NPP, 28% more PON export to the benthos, 20% more sedimentary

nitrification, and 30% more denitrification than in years with more MIZ production (Payne & Arrigo, 2022; Payne et al., 2021). However, in the south, only 10 years featured moderate UIBs, and even in those years, the OW period contributed more to annual NPP. Instead, NPP during the far-longer OW period (~5 months) drove the much higher rates of annual NPP, PON export to the benthos, and sedimentary nitrification and denitrification observed in the south. Moreover, while annual NPP, PON export to the benthos, and sedimentary nitrification and denitrification all decreased over time in the northern Chukchi Sea, there were no secular changes between 1988 and 2018 in the south. Instead, interannual variation in PON export to the benthos and sedimentary nitrification and denitrification were driven by a decline in NPP in the autumn (September and October) as a result of enhanced autumn stratification between 1988 and 2018.

4.3. The Future Chukchi Sea

Both the trends in sea ice cover observed over the past 40 years (Kwok, 2018; Lewis et al., 2020; Serreze et al., 2016; Serreze & Stroeve, 2015) and modeling studies (Wang & Overland, 2015) indicate that the Arctic Ocean is shifting to a state more like the southern Chukchi Sea of today, with thin, first-year ice that melts early, allowing a long OW period each summer. Pan-Arctic modeling studies indicate that thus far, a longer OW period has corresponded to an increase in NPP (Clement Kinney et al., 2020; Jin et al., 2016; Zhang et al., 2015). As the Chukchi Sea experiences a longer OW period, our results indicate that annual NPP in the north could increase by over 25%, which could result in ~50% more sedimentary denitrification. Even though the Chukchi Sea has historically been responsible for 1%–3% of the global loss of fixed N in the oceans (Chang & Devol, 2009), our results indicate that a transition to a much longer ice-free period in the region will increase the rate of denitrification in the sediments, resulting in a greater loss of fixed N. As larger phytoplankton blooms take up a greater proportion of the available NO_3^- in the Chukchi Sea, the amount of NO_3^- available in N-limited waters downstream will be reduced (Arrigo & Van Dijken, 2015). This may already be happening; satellite analysis revealed that in years following unusually high NPP in the Chukchi Sea, there was a significant reduction in NPP downstream in the Greenland Sea (Arrigo & Van Dijken, 2015).

A reduction in the NPP of ecosystems downstream of the Chukchi Sea could reduce the abundance of zooplankton, fish, marine mammals, and seabirds that rely on phytoplankton blooms as a food source (Hamilton et al., 2021; Joiris, 2011; Munk, 2003; Rysgaard et al., 1999). Additionally, increasing N removal through denitrification in the Chukchi Sea would exacerbate the low ratio of available N:P (phosphorus) found on the Chukchi shelf (Deutsch & Weber, 2012; Devol et al., 1997; Gruber & Sarmiento, 1997; Mills et al., 2015). The Chukchi shelf currently contains some of the world's lowest values of N* (a measure of excess N relative to phosphorus; Gruber & Sarmiento, 1997) in the global ocean (Deutsch & Weber, 2012). Yamamoto-Kawai et al. (2006) found that high rates of N_2 fixation in the surface waters of the North Atlantic were stimulated by the lower N:P ratios emanating from upstream in the Chukchi Sea, indicating that higher rates of NPP and greater denitrification in the future might further increase rates of N_2 fixation in waters downstream of the Chukchi Sea. Finally, there is increasing evidence that low N* values may even stimulate N_2 fixation in the Arctic Ocean (Blais et al., 2012; Díez et al., 2012; Fernández-Méndez et al., 2016; Moisander et al., 2010; Mulholland et al., 2012; Tremblay & Gagnon, 2009). Although data are sparse, Sipler et al. (2017) found that rates of N_2 fixation in the Arctic Ocean may currently offset up to 27% of the N deficit driven by denitrification in Arctic sediments.

While our results demonstrate that a shift toward a longer, more productive OW season could enhance denitrification, they also highlight that the UI period may not remain dominant in the northern Chukchi Sea in the future. Modeling efforts to assess the importance of UIBs have demonstrated that these blooms have increased in magnitude in the northern Chukchi Sea by 2% per year between 1988 and 2013 (Zhang et al., 2015) and by over 5% per year between 1980 and 2018 in the central Arctic (Clement Kinney et al., 2020). The radiative transfer model of Horvat et al. (2017) further indicates that between 2006 and 2015, 30% of the Arctic Ocean received sufficient light to allow for UI phytoplankton growth for at least three days in July. However, in comparing three other models, Jin et al. (2016) found that the proportion of NPP generated in UIBs diminished between 1980 and 2009 on a pan-Arctic scale due to declines in sea ice cover over this period, suggesting a shift towards Subarctic ecosystems. The impacts of a shift away from UIBs would likely be substantial. When these massive blooms are generated, they can strip the surface ocean of nutrients at a time when water temperatures are below −1.5°C (Arrigo et al., 2012, 2014) and when zooplankton grazing is minimal (Campbell et al., 2001; Huntley & Lopez, 1992; Payne et al., 2021). This may substantially reduce pelagic food availability for the fish, birds,

and mammals that feed in the Chukchi Sea (Bradstreet & Cross, 1982; Loeng et al., 2005) while simultaneously increasing benthic-pelagic coupling, benthic production, and enhancing sedimentary denitrification and fixed N loss. However, the waning magnitude of UIBs in the south suggests that these blooms may only affect the biogeochemistry of the Chukchi Sea and downstream waters for a few more decades.

Data Availability Statement

All model input and output data are available at https://purl.stanford.edu/nz800dp6262.

Acknowledgments
The authors would like to thank Matthew Mills and Stephanie Lim for providing input on analysis.

References

Ardyna, M., Babin, M., Gosselin, M., Devred, E., Rainville, L., & Tremblay, J.-É. (2014). Recent Arctic Ocean sea ice loss triggers novel fall phytoplankton blooms. *Geophysical Research Letters*, *41*, 6207–6212. https://doi.org/10.1002/2014GL061047

Arrigo, K. R. (2017). Sea ice as a habitat for primary producers. In D. N. Thomas (Ed.), *Sea ice* (pp. 352–369). John Wiley & Sons, Ltd. https://doi.org/10.1002/9781118778371.ch14

Arrigo, K. R., Mills, M., Van Dijken, G. L., Lowry, K., Pickart, R., & Schlitzer, R. (2017). Late spring nitrate distributions beneath the ice-covered northeastern Chukchi shelf. *Journal of Geophysical Research: Biogeosciences*, *122*, 2409–2417. https://doi.org/10.1002/2017JG003881

Arrigo, K. R., Perovich, D. K., Pickart, R. S., Brown, Z. W., Van Dijken, G. L., Lowry, K. E., et al. (2012). Massive phytoplankton blooms under Arctic sea ice. *Science*, *336*, 1408. https://doi.org/10.1126/science.1215065

Arrigo, K. R., Perovich, D. K., Pickart, R. S., Brown, Z. W., Van Dijken, G. L., Lowry, K. E., et al. (2014). Phytoplankton blooms beneath the sea ice in the Chukchi Sea. *Deep-Sea Research Part II Topical Studies in Oceanography*, *105*, 1–16. https://doi.org/10.1016/j.dsr2.2014.03.018

Arrigo, K. R., & Van Dijken, G. L. (2011). Secular trends in Arctic Ocean net primary production. *Journal of Geophysical Research: Oceans*, *116*(9), 1–15. https://doi.org/10.1029/2011JC007151

Arrigo, K. R., & Van Dijken, G. L. (2015). Continued increases in Arctic Ocean primary production. *Progress in Oceanography*, *136*, 60–70. https://doi.org/10.1016/j.pocean.2015.05.002

Assmy, P., Ehn, J. K., Fernández-Méndez, M., Hop, H., Katlein, C., Sundfjord, A., et al. (2013). Floating ice-algal aggregates below melting Arctic sea ice. *PLoS One*, *8*(10), e76599. https://doi.org/10.1371/journal.pone.0076599

Blais, M., Tremblay, J.-É., Jungblut, A. D., Gagnon, J., Martin, J., Thaler, M., & Lovejoy, C. (2012). Nitrogen fixation and identification of potential diazotrophs in the Canadian Arctic. *Global Biogeochemical Cycles*, *26*(3), 2011GB004096. https://doi.org/10.1029/2011GB004096

Bradstreet, M. S., & Cross, W. E. (1982). Trophic relationships at high Arctic ice edges. *Arctic*, *35*(1), 1–12. https://doi.org/10.14430/arctic2303

Brown, Z. W., Casciotti, K. L., Pickart, R. S., Swift, J. H., & Arrigo, K. R. (2015). Aspects of the marine nitrogen cycle of the Chukchi Sea shelf and Canada Basin. *Deep-Sea Research Part II Topical Studies in Oceanography*, *118*, 73–87. https://doi.org/10.1016/j.dsr2.2015.02.009

Burchard, H., Bolding, K., & Ruiz-Villarreal, M. (1999). *GOTM, a general ocean turbulence model. Theory, implementation and test cases*. Space Applications Institute.

Campbell, R. G., Wagner, M., Teegarden, G., Boudreau, C., & Durbin, E. (2001). Growth and development rates of the copepod *Calanus finmarchicus* reared in the laboratory. *Marine Ecology Progress Series*, *221*, 161–183. https://doi.org/10.3354/meps221161

Chang, B. X., & Devol, A. H. (2009). Seasonal and spatial patterns of sedimentary denitrification rates in the Chukchi Sea. *Deep-Sea Research Part II Topical Studies in Oceanography*, *56*(17), 1339–1350. https://doi.org/10.1016/j.dsr2.2008.10.024

Clement Kinney, J., Maslowski, W., Osinski, R., Jin, M., Frants, M., Jeffery, N., & Lee, Y. J. (2020). Hidden production: On the importance of pelagic phytoplankton blooms beneath Arctic sea ice. *Journal of Geophysical Research: Oceans*, *125*(9). https://doi.org/10.1029/2020JC016211

Cooper, L. W., & Grebmeier, J. M. (2018). Deposition patterns on the Chukchi shelf using radionuclide inventories in relation to surface sediment characteristics. *Deep-Sea Research Part II: Topical Studies in Oceanography*, *152*, 48–66. https://doi.org/10.1016/j.dsr2.2018.01.009

Corlett, W. B., & Pickart, R. S. (2017). Progress in oceanography the Chukchi slope current. *Progress in Oceanography*, *153*, 50–65. https://doi.org/10.1016/j.pocean.2017.04.005

Davis, J., & Benner, R. (2007). Quantitative estimates of labile and semi-labile dissolved organic carbon in the western Arctic Ocean: A molecular approach. *Limnology & Oceanography*, *52*(6), 2434–2444. https://doi.org/10.4319/lo.2007.52.6.2434

Deutsch, C., & Weber, T. (2012). Nutrient ratios as a tracer and driver of ocean biogeochemistry. *Annual Review of Marine Science*, *4*(1), 113–141. https://doi.org/10.1146/annurev-marine-120709-142821

Devol, A. H., Codispoti, L. A., & Christensen, J. P. (1997). Summer and winter denitrification rates in western Arctic shelf sediments. *Continental Shelf Research*, *17*(9), 1029–1033. https://doi.org/10.1016/s0278-4343(97)00003-4

Díez, B., Bergman, B., Pedrós-Alió, C., Antó, M., & Snoeijs, P. (2012). High cyanobacterial nifH gene diversity in Arctic seawater and sea ice brine: Arctic nifH gene diversity. *Environmental Microbiology Reports*, *4*(3), 360–366. https://doi.org/10.1111/j.1758-2229.2012.00343.x

Dupont, F. (2012). Impact of sea-ice biology on overall primary production in a biophysical model of the pan-Arctic Ocean: Arctic ice-ocean bio-physical model. *Journal of Geophysical Research: Oceans*, *117*(C8). https://doi.org/10.1029/2011jc006983

Fernández-Méndez, M., Turk-Kubo, K. A., Buttigieg, P. L., Rapp, J. Z., Krumpen, T., Zehr, J. P., & Boetius, A. (2016). Diazotroph diversity in the sea ice, melt ponds, and surface waters of the Eurasian basin of the central Arctic Ocean. *Frontiers in Microbiology*, *7*. https://doi.org/10.3389/fmicb.2016.01884

Fortier, M., Fortier, L., Michel, C., & Legendre, L. (2002). Climatic and biological forcing of the vertical flux of biogenic particles under seasonal Arctic sea ice. *Marine Ecology Progress Series*, *225*, 1–16. https://doi.org/10.3354/meps225001

Gosselin, M., Levasseur, M., Wheeler, P. A., Horner, R. A., & Booth, B. C. (1997). New measurements of phytoplankton and ice algal production in the Arctic Ocean. *Deep-Sea Research Part II: Topical Studies in Oceanography*, *44*(8), 1623–1644. https://doi.org/10.1016/S0967-0645(97)00054-4

Gradinger, R. (1996). Occurrence of an algal bloom under Arctic pack ice. *Marine Ecology Progress Series*, *131*(1–3), 301–305. https://doi.org/10.3354/meps131301

Gradinger, R. (2009). Sea-ice algae: Major contributors to primary production and algal biomass in the Chukchi and Beaufort Seas during May/June 2002. *Deep-Sea Research Part II: Topical Studies in Oceanography*, *56*(17), 1201–1212. https://doi.org/10.1016/j.dsr2.2008.10.016

Granger, J., Sigman, D. M., Gagnon, J., Tremblay, J.-E., & Mucci, A. (2018). On the properties of the Arctic halocline and deep water masses of the Canada Basin from nitrate isotope ratios. *Journal of Geophysical Research: Oceans*, *123*(8), 5443–5458. https://doi.org/10.1029/2018JC014110

Grebmeier, J. M. (2012). Shifting patterns of life in the Pacific Arctic and sub-Arctic seas. *Annual Review of Marine Science*, *4*, 63–78. https://doi.org/10.1146/annurev-marine-120710-100926

Grebmeier, J. M. (2017). The Distributed Biological Observatory (DBO) Conductivity-Temperature-Depth (CTD) data from 2011. DataOne Plus. [Dataset]. https://doi.org/10.18739/A29Z90C7B

Grömping, U. (2006). Relative importance for linear regression in *R*: The package relaimpo. *Journal of Statistical Software*, *17*(1). https://doi.org/10.18637/jss.v017.i01

Gruber, N., & Sarmiento, J. L. (1997). Global patterns of marine nitrogen fixation and denitrification. *Global Biogeochemical Cycles*, *11*(2), 235–266. https://doi.org/10.1029/97GB00077

Hameedi, M. J. (1978). Aspects of water column primary productivity in the Chukchi Sea during summer. *Marine Biology*, *48*(1), 37–46. https://doi.org/10.1007/BF00390529

Hamilton, C., Lydersen, C., Aars, J., Biuw, M., Boltunov, A., Born, E., et al. (2021). Marine mammal hotspots in the Greenland and Barents Seas. *Marine Ecology Progress Series*, *659*, 3–28. https://doi.org/10.3354/meps13584

Hill, V. J., Ardyna, M., Lee, S. H., & Varela, D. E. (2018). Decadal trends in phytoplankton production in the Pacific Arctic Region from 1950 to 2012. *Deep-Sea Research Part II: Topical Studies in Oceanography*, *152*, 82–94. https://doi.org/10.1016/j.dsr2.2016.12.015

Hill, V. J., & Cota, G. (2005). Spatial patterns of primary production on the shelf, slope, and basin of the western Arctic in 2002. *Deep-Sea Research Part II Topical Studies in Oceanography*, *52*(24–26), 3344–3354. https://doi.org/10.1016/j.dsr2.2005.10.001

Hill, V. J., Light, B., Steele, M., & Zimmerman, R. C. (2018). Light availability and phytoplankton growth beneath Arctic sea ice: Integrating observations and modeling. *Journal of Geophysical Research: Oceans*, *123*(5), 3651–3667. https://doi.org/10.1029/2017JC013617

Horvat, C., Jones, D. R., Iams, S., Schroeder, D., Flocco, D., & Feltham, D. (2017). The frequency and extent of sub-ice phytoplankton blooms in the Arctic Ocean. *Science Advances*, *3*(3). https://doi.org/10.1126/sciadv.1601191

Huntley, M., & Lopez, M. (1992). Temperature-dependent production of marine copepods: A global synthesis. *The American Naturalist*, *140*(2), 201–242. https://doi.org/10.1086/285410

Jin, M., Deal, C., Lee, S. H., Elliott, S., Hunke, E., Maltrud, M., & Jeffery, N. (2012). Investigation of Arctic sea ice and ocean primary production for the period 1992–2007 using a 3-D global ice-ocean ecosystem model. *Deep-Sea Research Part II: Topical Studies in Oceanography*, *81–84*, 28–35. https://doi.org/10.1016/j.dsr2.2011.06.003

Jin, M., Popova, E. E., Zhang, J., Ji, R., Pendleton, D., Varpe, Ø., et al. (2016). Ecosystem model intercomparison of under-ice and total primary production in the Arctic Ocean. *Journal of Geophysical Research: Oceans*, *121*(1), 934–948. https://doi.org/10.1002/2015JC011183

Joiris, C. R. (2011). A major feeding ground for cetaceans and seabirds in the south-western Greenland Sea. *Polar Biology*, *34*(10), 1597–1607. https://doi.org/10.1007/s00300-011-1022-1

Kwok, R. (2018). Arctic sea ice thickness, volume, and multiyear ice coverage: Losses and coupled variability (1958–2018). *Environmental Research Letters*, *13*, 105005. https://doi.org/10.1088/1748-9326/aae3ec

Lalande, C., Grebmeier, J. M., Hopcroft, R. R., & Danielson, S. L. (2020). Annual cycle of export fluxes of biogenic matter near Hanna Shoal in the northeast Chukchi Sea. *Deep-Sea Research Part II: Topical Studies in Oceanography*, *177*, 104730. https://doi.org/10.1016/j.dsr2.2020.104730

Laney, S. R., & Sosik, H. M. (2014). Phytoplankton assemblage structure in and around a massive under-ice bloom in the Chukchi Sea. *Deep-Sea Research Part II: Topical Studies in Oceanography*, *105*, 30–41. https://doi.org/10.1016/j.dsr2.2014.03.012

Lewis, K. M., & Arrigo, K. R. (2020). Ocean color algorithms for estimating chlorophyll *a*, CDOM absorption, and particle backscattering in the Arctic Ocean. *Journal of Geophysical Research: Oceans*, *125*(6), e2019JC015706. https://doi.org/10.1029/2019JC015706

Lewis, K. M., Van Dijken, G. L., & Arrigo, K. R. (2020). Changes in phytoplankton concentration now drive increased Arctic Ocean primary production. *Science*, *369*(6500), 198–202. https://doi.org/10.1126/science.aay8380

Loeng, H., Brander, K., Carmack, E., Denisenko, S., Drinkwater, K., Hansen, B., et al. (2005). Marine systems. Arctic climate impact assessment.

Lowry, K. E., Van Dijken, G. L., & Arrigo, K. R. (2014). Evidence of under-ice phytoplankton blooms in the Chukchi Sea from 1998 to 2012. *Deep-Sea Research Part II Topical Studies in Oceanography*, *105*, 105–117. https://doi.org/10.1016/j.dsr2.2014.03.013

Martin, J., Tremblay, J.-É., Gagnon, J., Tremblay, G., Lapoussière, A., Jose, C., et al. (2010). Prevalence, structure and properties of subsurface chlorophyll maxima in Canadian Arctic waters. *Marine Ecology Progress Series*, *412*, 69–84. https://doi.org/10.3354/meps08666

Maslowski, W., Marble, D., Walczowski, W., Schauer, U., Clement, J. L., & Semtner, A. J. (2004). On climatological mass, heat, and salt transports through the Barents Sea and fram strait from a pan-Arctic coupled ice-ocean model simulation: Mass and property fluxes into the Arctic. *Journal of Geophysical Research: Oceans*, *109*(C3). https://doi.org/10.1029/2001JC001039

Mayot, N., Matrai, P., Ellingsen, I. H., Steele, M., Johnson, K., Riser, S. C., & Swift, D. (2018). Assessing phytoplankton activities in the seasonal ice zone of the Greenland sea over an annual cycle. *Journal of Geophysical Research: Oceans*, *123*(11), 8004–8025. https://doi.org/10.1029/2018JC014271

McMinn, A., Ashworth, C., & Ryan, K. (1999). Growth and productivity of Antarctic sea ice algae under PAR and UV irradiances. *Botanica Marina*, *42*(4). https://doi.org/10.1515/BOT.1999.046

Mills, M. M., Brown, Z. W., Lowry, K. E., Van Dijken, G. L., Becker, S., Pal, S., et al. (2015). Impacts of low phytoplankton NO^{3-}:PO_4^{3-} utilization ratios over the Chukchi shelf, Arctic Ocean. *Deep-Sea Research Part II: Topical Studies in Oceanography*, *118*, 105–121. https://doi.org/10.1016/j.dsr2.2015.02.007

Moisander, P. H., Beinart, R. A., Hewson, I., White, A. E., Johnson, K. S., Carlson, C. A., et al. (2010). Unicellular cyanobacterial distributions broaden the oceanic N2 fixation domain. *Science*, *327*(5972), 1512–1514. https://doi.org/10.1126/science.1185468

Moore, S. E., & Grebmeier, J. M. (2018). The distributed biological observatory: Linking physics to biology in the Pacific Arctic region + supplementary file (see article tools). *Arctic*, *71*(5). https://doi.org/10.14430/arctic4606

Mulholland, M. R., Bernhardt, P. W., Blanco-Garcia, J. L., Mannino, A., Hyde, K., Mondragon, E., et al. (2012). Rates of dinitrogen fixation and the abundance of diazotrophs in North American coastal waters between Cape Hatteras and Georges Bank. *Limnology & Oceanography*, *57*(4), 1067–1083. https://doi.org/10.4319/lo.2012.57.4.1067

Mundy, C. J., Gosselin, M., Ehn, J., Gratton, Y., Rossnagel, A., Barber, D. G., et al. (2009). Contribution of under-ice primary production to an ice-edge upwelling phytoplankton bloom in the Canadian Beaufort Sea. *Geophysical Research Letters*, *36*(17), L17601. https://doi.org/10.1029/2009GL038837

Munk, P. (2003). Changes in plankton and fish larvae communities across hydrographic fronts off west Greenland. *Journal of Plankton Research*, *25*(7), 815–830. https://doi.org/10.1093/plankt/25.7.815

Niebauer, H. (1991). Bio-physical oceanographic interactions at the edge of the Arctic ice pack. *Journal of Marine Systems*, *2*(1–2), 209–232. https://doi.org/10.1016/0924-7963(91)90025-P

Nishino, S., Kikuchi, T., Fujiwara, A., Hirawake, T., & Aoyama, M. (2016). Water mass characteristics and their temporal changes in a biological hotspot in the southern Chukchi Sea. *Biogeosciences*, *13*(8), 2563–2578. https://doi.org/10.5194/bg-13-2563-2016

Osborne, E., Richter-Menge, J., & Jeffries, M. (2018). Arctic report card 2018 (Tech. Rep.).
Oziel, L., Massicotte, P., Randelhoff, A., Ferland, J., Vladoiu, A., Lacour, L., et al. (2019). Environmental factors influencing the seasonal dynamics of spring algal blooms in and beneath sea ice in western Baffin Bay. *Elementa: Science of the Anthropocene*, *7*, 34. https://doi.org/10.1525/elementa.372
Pacini, A., Moore, G. W. K., Pickart, R. S., Nobre, C., Bahr, F., Våge, K., & Arrigo, K. R. (2019). Characteristics and transformation of Pacific winter water on the Chukchi Sea shelf in late spring. *Journal of Geophysical Research: Oceans*, *124*(10), 7153–7177. https://doi.org/10.1029/2019JC015261
Payne, C. M., & Arrigo, K. R. (2022). Increases in benthic particulate export and sedimentary denitrification in the northern Chukchi Sea tied to under-ice primary production. *Journal of Geophysical Research: Oceans*, *127*(2). https://doi.org/10.1029/2021JC018110
Payne, C. M., Bianucci, L., Van Dijken, G. L., & Arrigo, K. R. (2021). Changes in under-ice primary production in the Chukchi Sea from 1988 to 2018. *Journal of Geophysical Research: Oceans*, *126*(9), e2021JC017483. https://doi.org/10.1029/2021JC017483
Peralta-Ferriz, C., & Woodgate, R. A. (2015). Seasonal and interannual variability of pan-Arctic surface mixed layer properties from 1979 to 2012 from hydrographic data, and the dominance of stratification for multiyear mixed layer depth shoaling. *Progress in Oceanography*, *134*, 19–53. https://doi.org/10.1016/j.pocean.2014.12.005
Perrette, M., Yool, A., Quartly, G. D., & Popova, E. E. (2011). Near-ubiquity of ice-edge blooms in the Arctic. *Biogeosciences*, *8*(2), 515–524. https://doi.org/10.5194/bg-8-515-2011
Reeve, J. L., Hamme, R. C., & Williams, W. J. (2019). Tracing denitrification in the Canada Basin: N2 loss to the atmosphere on the Chukchi shelf and benthic inputs in deep waters. *Deep-Sea Research Part I: Oceanographic Research Papers*, *143*, 127–138. https://doi.org/10.1016/j.dsr.2018.11.003
Richter-Menge, J., Druckenmiller, M., & Jeffries, M. (Eds.). (2019). *Arctic report card 2019* (p. 100).
Rysgaard, S., Nielsen, T., & Hansen, B. (1999). Seasonal variation in nutrients, pelagic primary production and grazing in a high-Arctic coastal marine ecosystem, Young Sound, northeast Greenland. *Marine Ecology Progress Series*, *179*, 13–25. https://doi.org/10.3354/meps179013
Sakshaug, E. (2004). Primary and secondary production in the Arctic seas. In *The organic carbon cycle in the Arctic Ocean* (pp. 57–81). Springer. https://doi.org/10.1007/978-3-642-18912-8_3
Serreze, M. C., Crawford, A. D., Stroeve, J. C., Barrett, A. P., & Woodgate, R. A. (2016). Variability, trends, and predictability of seasonal sea ice retreat and advance in the Chukchi Sea. *Journal of Geophysical Research: Oceans*, *121*(10), 7308–7325. https://doi.org/10.1002/2016JC011977
Serreze, M. C., & Stroeve, J. (2015). Arctic sea ice trends, variability, and implications for seasonal ice forecasting. *Philosophical transactions of the Royal Society of London*. 20140159.
Sherr, E. B., & Sherr, B. F. (2009). Capacity of herbivorous protists to control initiation and development of mass phytoplankton blooms. *Aquatic Microbial Ecology*, *57*(3), 253–262. https://doi.org/10.3354/ame01358
Sherr, E. B., Sherr, B. F., & Hartz, A. J. (2009). Microzooplankton grazing impact in the western Arctic Ocean. *Deep-Sea Research Part II: Topical Studies in Oceanography*, *56*(17), 1264–1273. https://doi.org/10.1016/j.dsr2.2008.10.036
Shimada, K., Kamoshida, T., Itoh, M., Nishino, S., Carmack, E., McLaughlin, F., et al. (2006). Pacific Ocean inflow: Influence on catastrophic reduction of sea ice cover in the Arctic Ocean. *Geophysical Research Letters*, *33*(8), L08605. https://doi.org/10.1029/2005GL025624
Sipler, R. E., Gong, D., Baer, S. E., Sanderson, M. P., Roberts, Q. N., Mulholland, M. R., & Bronk, D. A. (2017). Preliminary estimates of the contribution of Arctic nitrogen fixation to the global nitrogen budget. *Limnology and Oceanography Letters*, *2*(5), 159–166. https://doi.org/10.1002/lol2.10046
Smetacek, V. (1999). Diatoms and the ocean carbon cycle. *Protist*, *150*(1), 25–32. https://doi.org/10.1016/S1434-4610(99)70006-4
Soetaert, K., Herman, P. M., & Middelburg, J. J. (1996b). A model of early diagenetic processes from the shelf to abyssal depths. *Geochimica et Cosmochimica Acta*, *60*(6), 1019–1040. https://doi.org/10.1016/0016-7037(96)00013-0
Soetaert, K., Herman, P. M. J., & Middelburg, J. J. (1996a). Dynamic response of deep-sea sediments to seasonal variations: A model. *Limnology & Oceanography*, *41*(8), 1651–1668. https://doi.org/10.4319/lo.1996.41.8.1651
Søreide, J. E., Leu, E. V., Berge, J., Graeve, M., & Falk-Petersen, S. (2010). Timing of blooms, algal food quality and Calanus glacialis reproduction and growth in a changing Arctic. *Global Change Biology*, *16*(11), 3154–3163. https://doi.org/10.1111/j.1365-2486.2010.02175.x
Stocker, T. F., Qin, D., Plattner, G.-K., Tignor, M. M. B., Allen, S. K., Boschung, J., et al. (2013). *Climate change 2013: The physical science basis* (Vol. 1535, p. 14). Cambridge University Press Cambridge.
Teal, L., Bulling, M., Parker, E., & Solan, M. (2008). Global patterns of bioturbation intensity and mixed depth of marine soft sediments. *Aquatic Biology*, *2*(3), 207–218. https://doi.org/10.3354/ab00052
Tremblay, J.-É., & Gagnon, J. (2009). The effects of irradiance and nutrient supply on the productivity of Arctic waters: A perspective on climate change. In J. C. J. Nihoul, & A. G. Kostianoy (Eds.), *Influence of climate change on the changing Arctic and sub-Arctic conditions* (pp. 73–93). Springer Netherlands. https://doi.org/10.1007/978-1-4020-9460-6_7
Waga, H., & Hirawake, T. (2020). Changing occurrences of fall blooms associated with variations in phytoplankton size structure in the Pacific Arctic. *Frontiers in Marine Science*, *7*, 209. https://doi.org/10.3389/fmars.2020.00209
Wang, M., & Overland, J. E. (2015). Projected future duration of the sea-ice-free season in the Alaskan Arctic. *Progress in Oceanography*, *136*, 50–59. https://doi.org/10.1016/j.pocean.2015.01.001
Woodgate, R. A. (2018). Increases in the Pacific inflow to the Arctic from 1990 to 2015, and insights into seasonal trends and driving mechanisms from year-round Bering Strait mooring data. *Progress in Oceanography*, *160*, 124–154. https://doi.org/10.1016/j.pocean.2017.12.007
Woodgate, R. A., Weingartner, T. J., & Lindsay, R. (2012). Observed increases in Bering Strait oceanic fluxes from the Pacific to the Arctic from 2001 to 2011 and their impacts on the Arctic Ocean water column. *Geophysical Research Letters*, *39*(24), 2012GL054092. https://doi.org/10.1029/2012GL054092
Yamamoto-Kawai, M., Carmack, E., & McLaughlin, F. (2006). Nitrogen balance and Arctic throughflow. *Nature*, *443*(7107), 43. https://doi.org/10.1038/443043a
Zhang, J., Ashjian, C., Campbell, R. G., Spitz, Y. H., Steele, M., & Hill, V. J. (2015). The influence of sea ice and snow cover and nutrient availability on the formation of massive under-ice phytoplankton blooms in the Chukchi Sea. *Deep-Sea Research Part II*, *118*, 122–135. https://doi.org/10.1016/j.dsr2.2015.02.008